High Gain Planar Antenna Structures for Ka-band Applications

Kiran Dnyandeo Phalak

A Thesis

in

The Department

Of

Electrical and Computer Engineering

Presented in Partial Fulfillment of the requirements

For the degree of Master in Applied Science (Electrical Engineering) at

Concordia University

Montreal, Quebec, Canada

April 2014

CONCORDIA UNIVERSITY
SCHOOL OF GRADUATE STUDIES

This is to certify that the thesis prepared

By: Kiran Dnyandeo Phalak

Entitled: "High Gain Planar Antenna Structures for Ka-band Applications"

and submitted in partial fulfillment of the requirements for the degree of

Master of Applied Science

Complies with the regulations of this University and meets the accepted standards with respect to originality and quality.

Signed by the final examining committee:

_____ Chair
         Dr. M. Z. Kabir

_____ Examiner, External
         Dr. H. Akbari, (BCEE)   To the Program

_____ Examiner
         Dr. T. Denidni

_____ Supervisor
         Dr. A. Sebak

Approved by: _____
                        Dr. W. E. Lynch, Chair
              Department of Electrical and Computer Engineering

_____20_____   _____
                                              Dr. C. W. Trueman
                                    Interim Dean, Faculty of Engineering
                                    and Computer Science

Abstract

High Gain Planar Antenna Structures for Ka-band Applications

Kiran Phalak

Antennas are an essential part of a communication system as they control a coverage area of the signal. The millimeter wave band has the potential to offer numerous radio applications which require the large bandwidth channels. Due to the current cellular subscribers' demand of higher data rates, even cellular communication is expected to move in millimeter wave communications at Ka band of 26.5 GHz to 40 GHz. However, millimeter waves are sensitive to the high degree of atmospheric and oxygen absorption losses. This challenge of the millimeter wave communication can be tackled by employing high gain antennas. In addition, modern electronic products require compact handheld devices to offer the user-friendly system as well as capture the market. Therefore, planar antenna structures are apt for these communication systems.

In this thesis, two antenna structures are presented at the Ka band for millimeter wave communications. Initially, four element patch antenna is presented for high gain in the broadside direction. Patch elements are excited using an aperture coupling from 50Ω microstrip line. Air-gap cavity is used to improve the impedance bandwidth of the design. This structure obtains a relatively moderate impedance bandwidth of 4.6%. The proposed four-element patch antenna exhibits a flat gain over an operating band with 13.8 dB gain at the design frequency. The antenna achieves a wide beamwidth of 70^0 in H plane. In addition, side lobe levels in E and H planes are -14.5 dB and 23 dB respectively. For the second prototype, an Antipodal Fermi-Linear Tapered Slot Antenna (AFLTSA) is presented to achieve the wide impedance bandwidth

with high flat gain for endfire radiation. Substrate Integrated waveguide (SIW) technique is utilized to feed the AFLTSA which reduces insertion losses of the structure. Fermi-Dirac distributed curve in conjunction with a linear curve for a tapered slot increases the coupling of the electric field from a substrate integrated waveguide to the tapered slot. Knife edge rectangular corrugation profile is used at edges of AFLTSA in order to reduce the side lobes and cross polarization levels of radiation pattern. The proposed structure achieves the wide impedance bandwidth to support requirements for high data rate channels. Measurement results from a fabricated prototype exhibit a flat gain over an entire operating frequency band with 16.4 dB gain at 28 GHz. The wide impedance bandwidth is achieved with return loss below 15 dB. Proposed structure has low side lobe levels of -13.9 dB in H plane and -19.5 dB in E plane. In addition, it offers a low cross polarization level of -22 dB.

Acknowledgement

First and foremost, I would like to convey my thanks to my supervisor Dr. Abdel Sebak for his guidance throughout this work. His timely consultation and advises have a huge part in framing this research work. I am grateful to him to offer the opportunity to work with him in the field of millimeter wave antenna designing.

My sincere thanks to Dr. Ahmed Kishk and Dr. Robert Paknys for their engrossing teaching and critical technical guidance about electromagnetics during the Master of Engineering program. I am thankful for my friend and PhD aspiring, Zouhair Briqech, for his collaboration with one of the important sections of this thesis work. His expertise and experience in an antenna fabrication and measurement systems has been more than handful for me to complete my work within time. I am gratified to get valuable tips and technical understanding from my fellow electromagnetic group students. I obliged to them for keeping the sportive atmosphere in the premises which helped me to focus and work ardently as well.

My graduation could not have happened without moral and all kind of support from my parents. I am deeply thankful to my brother for believing in my abilities and interest. Without their encouragement and support this would not have been possible.

Table of Contents

Chapter 1

Introduction---1

Chapter 2

Literature Overview---11

Chapter 3

Four Element Aperture Coupled Patch Antenna-------------------------------- 30

Chapter 4

Antipodal Fermi-Linear Tapered Slot Antenna------------------------------------46

Chapter 5

Conclusion--64

References---67

List of Abbreviations

AFLTSA   Antipodal Fermi Linear Tapered Slot Antenna

ALTSA   Antipodal Linear Tapered Slot Antenna

CAD   Computer Aided Design

CBCPW   Conductor Backed Coplanar waveguide

CDMA   Code Division Multiple Access

CEPT   European Conference of Postal and Telecommunications Administrations

CPW   Coplanar Waveguide

DRA   Dielectric Resonator Antenna

FCC   Federal Communications Commission

FEM   Finite Element Method

FIT   Finite Integration Technique

FM   Frequency Modulation

GCPW   Grounded Coplanar Waveguide

GPS   Global Positioning System

HF   High Frequency

HSPA   High Speed Package Access

ISM   Industrial Scientific Medical

ITU   International Telecommunication Union

LF   Low Frequency

LTCC   Low temperature co-fired ceramic

LTE   Long Term Evolution

LTSA   Linear Tapered Slot Antenna

LWA	Leaky Wave Antenna
MIC	Microwave Integrated Circuit
MIMO	Multiple Input Multiple Output
MMID	Millimeter Identification
MMW	Millimeter waves
PCB	Printed Circuit Board
PTFE	Poly Tetra Fluoro Ethylene
QTEM	Quasi Transverse Electromagnetic
RADAR	Radio Detection and Ranging
RFID	Radio Frequency Identification
SiP	System-in-Package
SIRC	Substrate Integrated Radial Coaxial
SIW	Substrate Integrated Waveguide
SoP	System-on-Package
TDMA	Time Division Multiple Access
TE	Transverse Electric
TM	Transverse Magnetic
TSA	Tapered Slot Antenna
UHF	Ultra High Frequency
UTD	Uniform Theory of Diffraction
VHF	Very High Frequency
VoIP	Voice over Internet Protocol
WPAN	Wireless Personal Area Network

List of Symbols

B	Magnetic flux density
BW	Bandwidth
c	Speed of light / speed of EM waves in free space
C	Channel capacity
E	Electric field intensity
f	Operating frequency
H	Magnetic field intensity
J	Electric current density
L_{ant}	Length of antenna
R	Distance between transmitter and receiver
S/N	Signal to noise ratio
ε_r	Relative permittivity
λ_g	Guided wavelength
λ_0	Free space wavelength
λ	Operating wavelength

List of Figures

List of Tables

Chapter 1
Introduction

1.1 Introduction to the Wireless Communication

Wireless communications have been a focus of researchers all over the globe ever since Marconi built the first radio system in 1895 [1]. Just a thought of transferring data from one place to another by means of oscillating electromagnetic waves, motivated researchers from various fields to explore the field of wireless data transfer. As a result, wireless data transfer is not only limited for a communication purpose, but also being used in medical, surveillance, amateur radio, robotics and radio broadcast fields' applications. One of the largest application of wireless communication is a cellular communication. Similarly, a satellite communication is also a major wireless field as it offers educational, security, communication advantages. Other examples include short distance wireless data transfer by the Bluetooth standard and radio frequency identification (RFID) that allows tracking as well as data acquisition from tagged remote objects [2]. Radio detection and ranging (RADAR) finds its way into military, air traffic control, and surveillance applications [3]. In the medical field, this principle is used for a cancer detection [4] and cardiac monitoring [5].

In general, wireless communication among points can be divided into three main stages, as shown in Fig. 1.1: transmission, propagation and reception. Transmission stage deals with processing of baseband or low frequency (LF) signal. A transmitter modulates LF data on a high frequency carrier signal and launches it in the space. A modulated signal propagates through the space in the form of electromagnetic waves. During the propagation, a signal deals with

turbulent man-made or natural noise sources which attenuates and deforms the signal. At the receiving end, this signal is captured by the receiver which filters out unwanted signals. The original data is recovered by the demodulation process at the receiver. As spurious effects during the propagation cannot be controlled, design of effective transmission and reception system is essential for reliable wireless communication [6].

Figure 1.1 Block diagram of wireless communication

At both ends of a wireless link, the task of radiating and capturing the electromagnetic energy in and from the desired direction is performed by an antenna. An antenna itself is a passive reciprocal device. Therefore, whenever a transmitting antenna is discussed, the discussion always implies for a receiving antenna as well, unless specifically stated. A performance of any antenna can be described by the values of its various parameters. Antenna parameters include directivity, efficiency, beamwidth, impedance bandwidth, side lobe level, polarization and input impedance [7]. In addition, cost, weight and size of antenna can also be critical for certain applications. Any handheld device operating on a battery, thus, needs a power efficient antenna such that its battery life will last longer. Satellite communication requires a narrow beam antenna whereas broadcast communication requires wide beam antennas. Dual polarization is required to establish two individual communication channels with the same antenna system. Hence, antenna design is solely dependent on the application in which it is to be used.

1.2 Motivation

1.2.1 Need for Millimeter Wave Communication

The rapid growth in radio communication industries and applications has clustered the electromagnetic spectrum. Therefore, wireless channel allocation in each country is regulated by national organizations such as Federal Communications Commission (FCC), Industry Canada, European Conference of Postal and Telecommunications Administrations (CEPT) [6]. Although this ensured that no chaos can be caused by the communication interference, scarcity of available wireless channels still continues to be a big challenge faced by wireless industries. As most of the current wireless systems operate at HF (3MHz to 30MHz), VHF (30MHz to 300MHz) and UHF (300MHz to 3GHz) bands, the electromagnetic spectrum at these bands is crowded [8]. In addition, the relative bandwidth of communication channels at these bands is in the range of few megahertz. According to Shannon–Hartley theorem, given by (1.1), a channel capacity (C) is directly dependent on the bandwidth (BW) of a communication channel and the signal to noise ratio (S/N) [9]. Therefore, applications which require higher data speed cannot operate satisfactorily at these low bandwidth channels.

$$C = BW \log_2(1 + S/N) \qquad (1.1)$$

The most logical solution for this problem is shifting wireless applications towards higher frequencies. Typically, the electromagnetic spectrum in the range of 30 GHz to 300 GHz (i.e. wavelength of 10 mm to 1 mm) is referred as the millimeter wave (MMW) frequency band. It can be also defined Extremely high frequency (EHF) band [3].

Millimeter wave characteristics have numerous advantages from the communication system point-of-view as discussed ahead:

- Smaller wavelengths allow the design of small size components, resulting in a compact system.

- For same physical size, narrow beamwidth can be obtained using MMW antennas as operating wavelength is smaller [3].

- The bandwidth available at MMW is extremely large, hence wide bandwidth channels can be allocated in MMW frequencies [10].

- Wide band spread spectrum capability for reduced multipath and clutter [3].

- Availability of certain high attenuation bands which has potential for highly secure short distance communication [10].

Along with advantages, MMW characteristics also exhibit certain disadvantages for communications applications.

- According to the Friis transmission equation, a free space loss factor, given in (1.2), increases with a square of the operating signal frequency [11].

$$free\ space\ loss\ factor = \left(\frac{4\pi R}{\lambda}\right)^2 = \left(\frac{4\pi f R}{c}\right)^2 \qquad (1.2)$$

- An atmospheric attenuation, caused by rain, scattering, water vapor and oxygen absorption at MMW frequency, limits the communication range [10].

- Smaller wavelength results in small component size, resulting in a necessity of highly precise production processing.

- Narrow beamwidth offered by MMW can be a problem for a large volume search radar [3].

Although MMW communication had much lesser exploitation than microwave communication, MMW communication has been utilized and proposed for following applications for many years [3][10].

1. Secure military communication

2. Radio astronomy and meteorological satellites

3. Weather and military radars

4. Millimeter wave imaging

5. Remote sensing applications

6. Gigabit wireless communications

7. Wireless HDTV

One of the biggest challenges of MMW communications is to reduce the cost of the system. As component size gets smaller at higher operating frequency range, processing techniques of this precision are expensive, resulting in high cost of complete systems. In addition, due to small wavelength MMW components are sensitive to edge diffraction as compared to microwave range components [12]. Furthermore, most of the standard values mentioned in datasheets of materials available in the market are given for microwave frequencies. Their properties differ from the specification which makes it challenging to design the MMW components. Various technologies which are being proposed at MMW are still to be well established in the industry. Last but not the least, the most fearsome challenge at MMW communication is ever increasing atmospheric attenuation. It is a challenge to design high gain antennas to nullify effects of the atmospheric attenuation [10].

Nevertheless, a detailed experimental study of a non-linearity of an atmospheric loss and research in modern technologies can help in tackling these challenges to utilize MMWs which

offer the large availability of communication channels with wide bandwidth. Hence, this thesis is concerned about antennas for the MMW communication and its application in an outdoor communication.

1.2.2 5G Cellular Communication at Ka band

Since early 1980s, when analog Frequency Modulation (FM) technology based cellular service was introduced as the first generation mobile communication system [13], the world has seen a rapid exponential growth in number mobile device users. Over four decades since the first generation was deployed, wireless communication industry has seen Time Division Multiple Access (TDMA), Code Division Multiple Access (CDMA), High Speed Packet Access (HSPA), Voice over Internet Protocol (VoIP) and Long Term Evolution (LTE) technologies which kept transforming cellular communication through various technological generations [14].
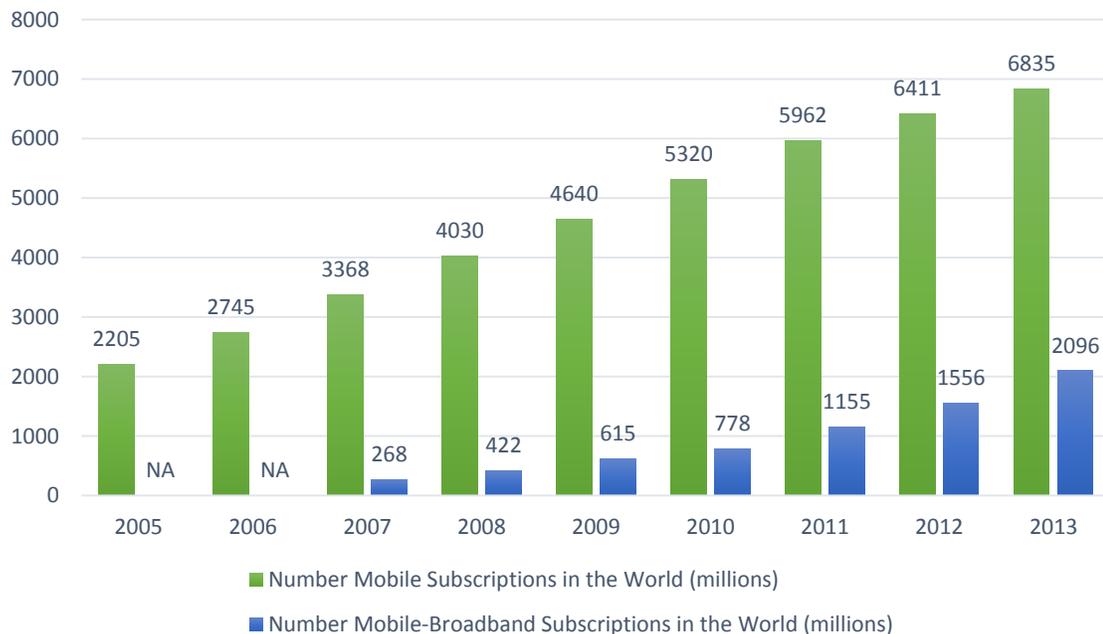
Figure 1.2 Rapid Growth in mobile subscribers [15] Source : ITU World Telecommunication/ICT Indicators database

Fig. 1.2[1] illustrates the rapid growth in the number of mobile subscriptions in the world during recent years. According to International Telecommunication Union (ITU) statistics, at the end of the year 2013, 96 mobile subscriptions for every 100 people in the world had been sold [15]. Although these numbers include both active and inactive cellular phone users [16], the rate of increase in the number of subscriptions is very high. This growth in the number of mobile subscribers increases the traffic of cellular signals all over the world which indicates saturation of radio spectrum currently allotted for cellular communication. Similarly, Fig. 1.2 also illustrates the rise in internet subscriptions on cellular phones i.e., mobile-broadband users. Smartphone applications such as global positioning system (GPS) tracking, live streaming of a high definition multimedia by broadband services on cellular devices has stimulated a ceaseless demand of a high speed cellular communication. This has also posed the challenge in front of a cellular industry to seek for higher bandwidth channels.

Use of MMWs can provide a solution for these challenges. Along with a wide bandwidth channels, MMW frequencies can bring in numerous communication advantages. Audio visual streaming can be provided with high data rate internet links as wide bandwidth channels with higher data capacity can be allotted. The unavoidable challenge of cellular signal traffic can be countered by allotting the large number of communication channels. MMWs have smaller wavelengths which allows technologies such as Multiple Input Multiple Output (MIMO) and adaptive beam forming to be utilized for reaching out for signals as well [14].

A general conception is that MMWs cannot be used for an outdoor line of sight (LOS) communication. The primary reason for this belief is free space path loss which is proportional

---

[1] Please note that mobile subscriptions refers to the number of SIM cards being used in each country, not the number of people using a mobile device. Some people have two mobile accounts on the go at a one time, possibly in two devices, possibly in a single dual-SIM device (which are becoming increasingly common in the developing world and are forecast by Strategy Analytics to reach 20 percent of handsets by 2016) [16].

to the square of the frequency [11]. In addition, the oxygen molecule absorption rate at MMWs is also high. However, in case of a cellular communication, microcells with a radius of approximately 200 meters are used in high traffic area. The study of an atmospheric attenuation at 200 meters from the transmitter, as shown in Fig. 1.3, reveals that 28 to 38 GHz frequencies demonstrate the low attenuation (0.04-0.07 dB/km) window [14]. Furthermore, attenuation due to heavy rain of 25 mm/hour, as shown in Fig. 1.4, at 28 GHz is approximately 1 dB for 200 meters [17].
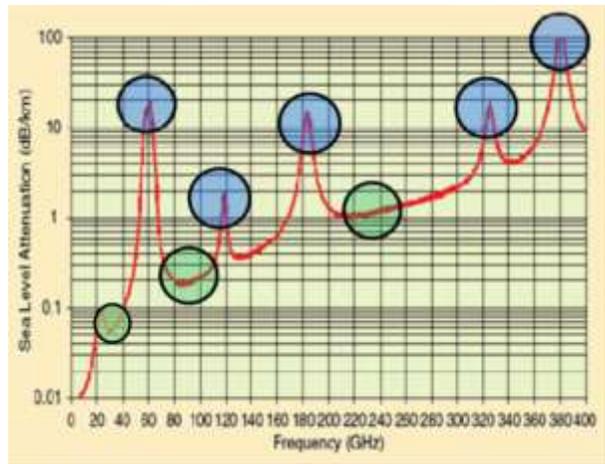
Figure 1.3 Atmospheric attenuation curve for millimeter waves [14]
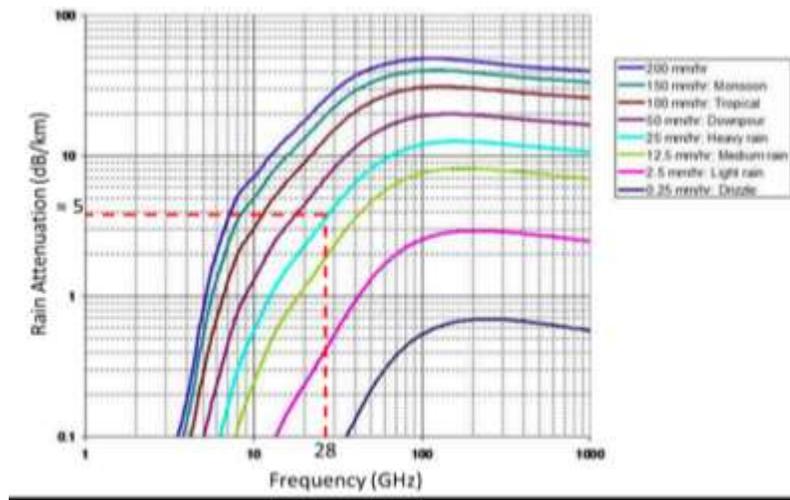
Figure 1.4 Rain attenuation curves for millimeter waves [18]

An antenna is an essential component to establish the wireless communication between two or more terminals. In case of cellular communication, base station antennas are used to offer coverage in cellular sectors. The principle function of base station antennas is to increase the coverage area. Therefore, critical design parameters for a cellular base station antenna are azimuth beamwidth and high gain. An azimuth angle is tilted from the normal towards the ground to improve the signal strength in a vicinity of the base station tower. This tilt in an azimuth angle can be achieved mechanically, electronically or by the combination of both [19]. High gain and wide beamwidth are required to achieve large coverage area. However, antenna beamwidth and gain are reciprocal to each other. Directivity of an antenna is typically increased by focusing the beam in narrow zone, hence the half power beam width is smaller. Therefore, multiple elements of high gain antenna are used to achieve this wide azimuth beamwidth [20].

These studies clearly identify the solution for a 5G cellular communication beyond 2025 lies with MMWs at 28 and 38 GHz. High gain, planar, low cost antenna structures are required for point-to-point or point-to-multipoint communication applications at Ka band of 26.5 GHz to 40 GHz.

1.3 Thesis Objective

This thesis is concerned about design of high gain compact antennas at Ka-band with focus on planar structures. The high gain requirement is mainly to address the atmospheric attenuation associated with MMW wireless communications. As cellular antenna structures operate in cell design structure, maximum front-to-back ratio is desired. Another objective of the thesis is to obtain a wide impedance bandwidth to support high data rate channels. Lower side lobe levels are desired as it will facilitate reduction in interference. The size of an antenna should be smaller so that it can be used in compact devices. Antenna elements are proposed for endfire and

broadside radiations. These elements can be used in a fixed multibeam array antenna to obtain the required azimuth bandwidth [20].

1.4 Thesis Organization

Chapter 2 reviews the literature of a millimeter wave communication from the early applications of a millimeter wave communication to its rise in various fields. The further section focuses on various technologies and antenna structures which are utilized to obtain high gain at MMWs. In depth discussion is also carried out for substrate integrated waveguide technology and tapered slot antenna technology which are utilized in this thesis. The chapter ends with a discussion on numerical techniques behind the simulation technology used for solving electromagnetic problems.

Chapter 3 presents the design of a broadside radiating four-element patch array antenna. Design methodology and working principle of the microstrip patch antenna are discussed. Furthermore, measurement results for this antenna are presented. Parametric study and simulation procedure are also discussed. The chapter concludes with comparison of results with previously proposed antenna structures.

Chapter 4 presents the endfire radiating antipodal fermi linear tapered slot antenna (AFLTSA). The design methodology is presented together with different parametric studies using full wave simulation CAD tools. An AFLTSA prototype and its measurement method and results are also presented. Simulated and measured results are compared.

Chapter 5 presents the conclusion of the thesis's work. It also recommends some future activities to be followed for completion of base station antenna design.

Chapter 2

Literature Overview

2.1 Evolution of Millimeter Wave Communication

Although the first MMW communication system had been designed by Jagadish chandra Bose before 1900 [21], it had not been popular for industrial or communication applications because only a large wavelength communication was preferred for long distance communication. Recent growth in the interest for the MMW communication has been triggered by the lack of available spectrum at lower frequencies. Furthermore, approximately 7 GHz of the unlicensed ISM band is allotted at 60 GHz millimeter waves in all countries [10]. Therefore, a large amount of the literature about MMW communication is focused at 60 GHz ISM band.

Early advancement in MMW communication had been in the area of RADAR applications. Smaller wavelength and narrow beamwidth, which could only be achieved at MMWs, were beneficial to obtain greater resolution with precision in target tracking, detection application. Additionally, it facilitates the higher angular resolution for area mapping application. The higher gain potential of high frequency antennas assists in detecting and locating small objects. At MMW, even a lower radial velocity of object results in higher Doppler shift. Hence, MMW radar has the higher detection capability for moving targets. MMW radars are used for military, weather forecast, air and marine traffic control, surveillance and radio astronomy applications [22].

Chipless millimeter wave identification (MMID) at 30 GHz was reported in [23]. At MMW, smaller size enables the design of a small tag antenna and a compact reader module as compare to the RFID system. Furthermore, chipless MMID reduces the cost of the system as a chip or integrated circuit is not required [23]. MMWs provide a deeper range than infrared or visible region as they penetrate through wood, clothes. Moreover, they provide better spatial resolution and compact system than microwave region. Therefore, MMWs are suitable for imaging applications [24]. Consequently, MMW imaging systems have also received a wide attention. In modern world of terrorist threats, MMW imaging can be used for a hidden object or weapon detection [25].

On the other hand, higher frequency, wide unlicensed band (of 7 GHz) and permission of high power transmission make 60 GHz MMW band most suitable for a gigabit wireless communication. IEEE standard 802.15.3C is 60 GHz multi-gigabit wireless personal area network (WPAN). Although the high attenuation rate at 60 GHz seems to be disadvantageous, in case of a short distance indoor communication, it facilitates the secure operation [10].

All these applications have forced modern materials and technologies to evolve in order to incorporate MMW communication as discussed in following sections of this chapter.

2.2 Antennas for Millimeter Wave Communication

MMW applications have created the demand for special components at MMW frequencies. To counter the propagation losses, high gain antennas are essential. In order to reduce the size, price and weight of the system, planar, low profile and low loss component design is desired. Due to smaller wavelength, MMW frequency operations require small component size, hence technologies and methods used at HF, VHF, and UHF range are generally not effective at MMW

frequencies. Discussion of various proposed modern technologies and antenna structures to obtain higher gain at MMW is carried out in the following sections.

2.2.1 Horn Antennas

Horn antenna is a case of aperture antennas. Traditionally, Horn antennas are utilized for obtaining the high gain and narrow beamwidth at microwaves and millimeter waves [11]. High gain along with a symmetric radiation pattern can be obtained by employing hard or soft surface in metallic horn antennas [26]. Machining of these metallic horn antennas at MMW is difficult and expensive. In addition, ohmic losses in metallic waveguide increase as a cross section of horn antenna decreases [27]. Furthermore, heavy, bulky structure of horn antennas makes them unsuitable to be employed in portable devices.
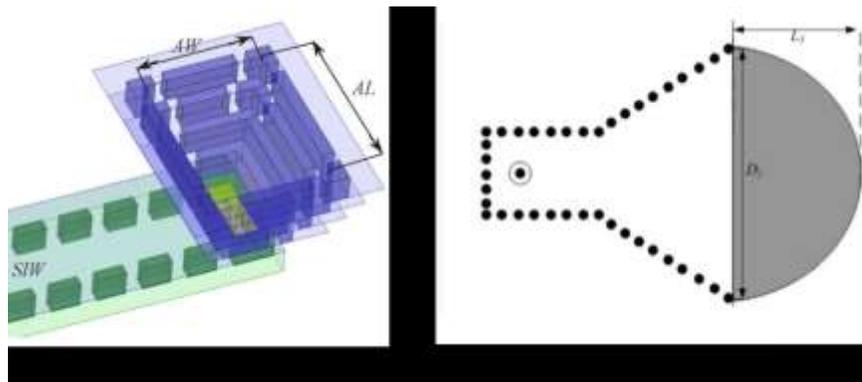
Figure 2.1 MMW horn antenna designs for (a) broadside radiation [28] and (b) endfire radiation [29]

Instead of a waveguide, other antenna structures are proposed to feed the horn shape for MMW applications to obtain the reduction in a weight. A balanced fed patch is used to feed the horn antenna for the design proposed in [30]. The multilayer pyramidal horn is designed using the PCB process at MMWs in [28]. In this structure, substrate integrated waveguide with transverse slots is used to feed the horn. This antenna structure could reach the gain of 12 dB. Similar work is discussed in [21] where a hybrid (patch and horn) antenna is designed for a

broadside radiation. However, horn shape in a broadside direction results in the non-planar structure.

Typically, the horn is a non-planar structure and used for an endfire radiation. Planar horns have been attempted for MMW applications using a substrate integration technology. Flared substrate integrated waveguide (SIW) can be used to construct the planar horn structure. Coplanar waveguide (CPW) fed planar horn antenna is designed in [31] using the modern micro fabrication procedure. In [32], waveguide feeding is used to make an H plane horn using PCB process. Waveguide fed structure achieved in a gain of about 5-6 dB without loading due to dielectric losses. In order to reduce the size of the structure, coaxial probe fed planar H plane horn is designed in [33] based on half mode substrate integrated waveguide (HMSIW) technology. It uses the principle of an electromagnetic field symmetry inside the waveguide. However, the dielectric filled structure obstructs the propagation of electromagnetic waves through the horn, resulting in reduction of gain. Therefore, attempts to design planar H-plane horn using special Poly Tetra Fluoro Ethylene (PTFE) substrate [34] or air [35] as a substrate have been made. Dielectric loading for a gain enhancement of H-plane horns are proposed in [36] and [29]. Nevertheless, dielectric field planar horns exhibited gain from 5-8 dB with a compact size in all these designs [29]-[36].

2.2.2 Lens Antennas

In order, to boost the gain of antenna elements, passive lenses are used ahead of moderate gain antenna structures. At the very high frequency range, electromagnetic waves can be treated as optical rays. At MMWs, the wavelength of the signal is very small, therefore lens antennas are analyzed using a geometrical optics [10]. Term lens has been interchangeably used for dielectric loading as well, in which case antenna substrate is extended in elliptical or random shape to

increase the gain of the structure [37]. The basic function of a dielectric lens is to transform a spherical or cylindrical wavefront of an antenna element radiation into a planar wavefront to achieve higher gain and narrow beamwidth [3]. When incident waves face the discontinuity between the dielectric medium of lens and air, part of incident rays are transmitted and partially they get refracted. In case of a convex lens, waves coming from a focal point bend towards the normal of the surface. Many lens techniques, shapes and materials had been investigated in the literature for millimeter wave antennas [10].
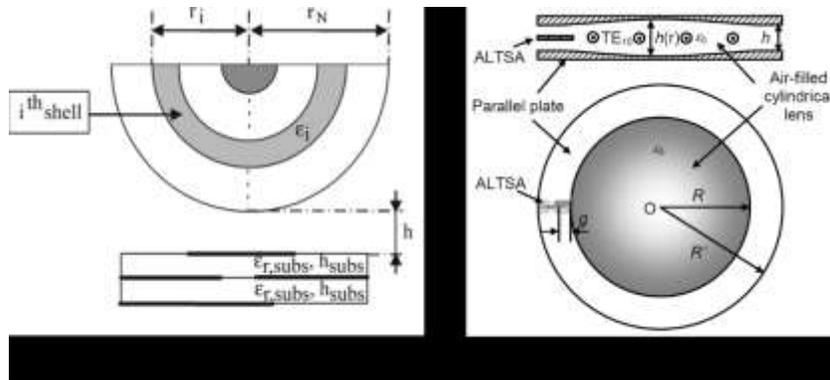
Figure 2.2 (a) half Maxwell fish-eye [38] and (b) Luneberg [39] lens antenna structures for MMW applications

Modified shaped cylindrical Luneberg lens antenna was presented for a front directed high gain. This structure used a parallel plate technique. It has two parallel plates separated by air, in which, the distance between the plates is varied to achieve the luneberg distribution in refractive index of a lens [39]. Similarly, high gain is achieved using a mechanically steered lens antenna for 60 GHz system. It has a circular horn followed by steerable hemispherical shaped dielectric lens to achieve the beam control [40]. In addition, [38] proposed half Maxwell fish-eye shaped antenna for a broadside radiation. It uses a multilayer lens structure with gradient-index. In this structure, different shells with individual dielectric constants are used which allows omnidirectional radiation pattern. Most part of ohmic losses in lens antennas are contributed by the feed element, as a lens itself does not contribute in ohmic losses in a great deal. Although

these lens systems exhibit the high gain about 18-20 dB, use of lens makes the system bulky and non-planar [39][40][38].

2.2.3 Dielectric Rod Antennas

Machining of metals is difficult, on the contrary, dielectrics are easy to machine and light weight. Therefore, dielectric based antennas received the attention for MMW applications. Frequently, the dielectric rod antenna had been proposed to achieve the endfire radiation. Dielectric rods are easy to design and low cost antennas.

The radiation behavior of the dielectric rod antenna can be explained by the discontinuity radiation concept [41] in which the antenna is regarded as an array composed of two effective sources at the feed and the free end of the rod. Part of the power excited at the feed is converted into guided-wave power, and is transformed into radiation power at the free (open) end. The remaining power is converted into unguided-wave power radiating near the feed end. Thus, the directivity of the dielectric rod antenna is characterized by the directivities generated by these two effective sources. However, there is the problem of quantitatively computing the radiation fields generated from the discontinuities at the feed and free ends [10].
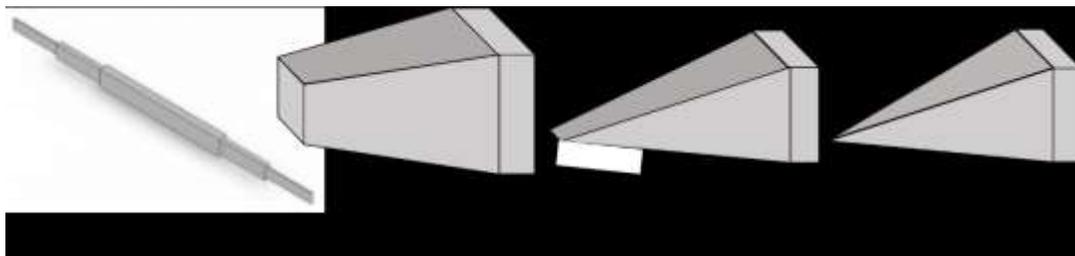
Figure 2.3 Different shapes of dielectric rod antennas (a) step tapered [42] (b) flat top (c) H plane tapered (d) E and H Plane tapered dielectric rods

Although dielectric rods are typically used for endfire radiation, if dielectric rod is loaded with metal strips, it can also be used for an omnidirectional radiation [43]. Linearly tapered [44] or

step tapered [42] dielectric rod antennas were extensively used as they provide an architecture which is easily integrated with miniature waveguide systems [45]. It has also been observed that a pointed dielectric rod has better performance than flat top dielectric rod antennas [44]. Variations of cylindrical dielectric rod antennas analyzed and utilized for array design in [46]. However, rods achieve moderate gain and offer the non-planar structures [42]-[46].

2.2.4 Slot Antennas
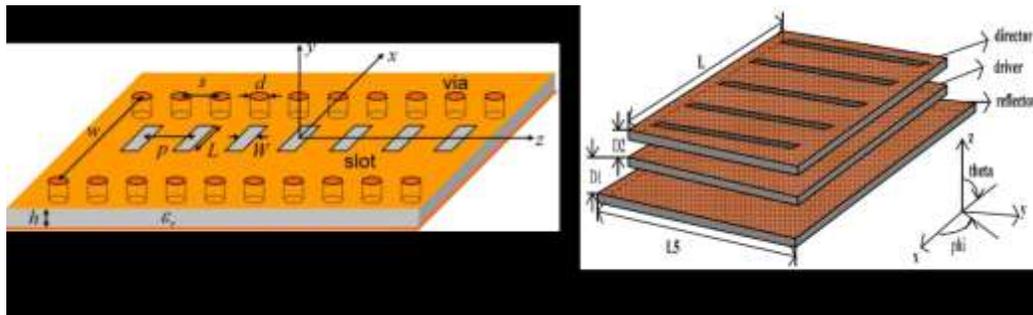
Figure 2.4 Slot antenna structures: (a) transverse slots on substrate integrated waveguide [47] and (b) slot director to enhance radiation pattern [48]

When a guided structure is loaded with perturbations, guiding wave propagating through structure excites radiating leaky wave from the structure. Leaky wave antennas (LWAs) such as slotted waveguide [49][50] had been in use for millimeter wave applications. When some type of asymmetry is introduced in a cross section of a guided structure, it causes radiation by the aperture. The degree of asymmetry will control the leakage rate and in turn the amplitude along the line source [50]. These antenna structures use costly, heavy and bulky waveguide structures as compared to the compact size of modern wireless application devices [47]. Furthermore, higher ohmic losses are present due to the metallic structure.

Planar substrate integrated waveguide slot antenna for a broadside radiation had been proposed in [47]. In this design, a periodic set of transverse slots are etched on a planar substrate integrated waveguide to obtain the broadside radiation. In this design spacing

between the consecutive slots decides the maxima direction of the radiation pattern. However, an ohmic loss analysis of this design shows that the conductor loss of slotted SIW is larger than the conductor loss of a corresponding closed rectangular waveguide. This is due to the fact that the current must bend around the slots, increasing the current density surrounding the slots, resulting in increased conductor loss [47].

Similar to yagi-uda antenna structure, directors ahead of slot structure are proposed in [48] to obtain the high gain in a broadside direction. It uses single layer 1, 3 or 5 slot directors to enhance the gain. However, introducing the directors and reflectors in either side of principle slot structure results in a bigger antenna structure.

2.2.5 Dielectric Resonator Antennas (DRA)
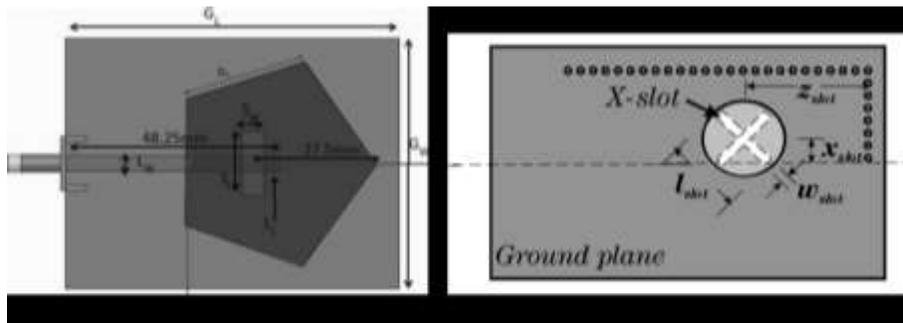
Figure 2.5 (a) Pentagonal [51] and (b) cylindrical [52] dielectric resonator antenna structures

Dielectric resonator antennas are used for MMW communication as broadside radiating elements. They are superior in terms of low ohmic losses, low dissipation. No surface waves in the DRA structures make them suitable for array designing where no mutual coupling between elements makes designing easier. Pentagon shaped aperture coupled dielectric resonator antenna is presented in [51]. It uses dielectric pentagon over an aperture to focus the radiation in broadside direction. In this design, aperture coupling from microstrip line is used to excite the dielectric resonator. One of the attraction of DRAs is their shape, it can assume cylindrical [52],

cubical [53], pentagonal [51] shape according to the available size without affecting the radiation pattern characteristics. However, if the height of dielectric resonator is significant, it results in a non-planar, high profile antenna structure.

2.2.6 Microstrip Antennas
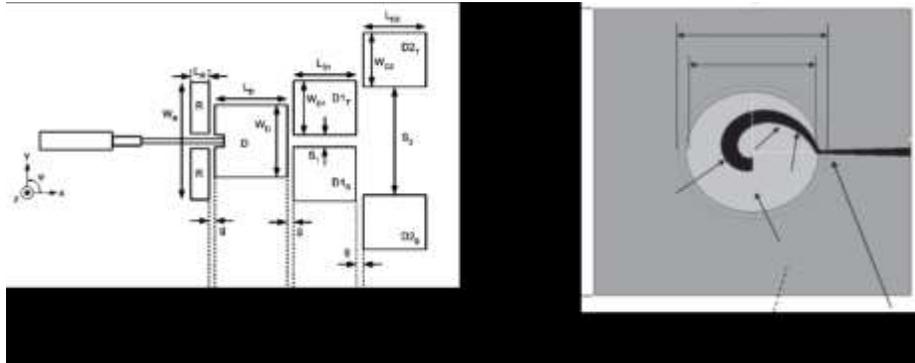
Figure 2.6 Microstrip antenna structures : (a) Yagi array [54] and (b) circular polarized microstrip antenna [55]

As a printed circuit board (PCB) technology is cheaper, printed antennas are getting extensively explored for MMW applications. A unique design for the printed yagi array antenna is presented in [54] for endfire radiation. Gain of above 10 dB is achieved with the use of multiple directors. This designed had been further improved using two layer structure and reflector patches in [56]. In [55], printed microstrip line antenna presented for circular polarization and high gain of 10 dB. Likewise, twin dipole [57], stacked patch [58], vertical patch [59] antennas are proposed using printed circuit boards to achieve high gain at MMW antennas. Losses are present due to dielectric substrate and surface waves in the microstrip antennas. In case of array structures, power divider circuits contribute in ohmic losses in great deal. Although ohmic losses due to copper layer increase at MMW, using low profile substrates and thin copper layer have shown the total efficiency of 95% being achieved [56]. In addition, there planar and cheaper structure along with ability to achieve the high gain make them suitable for modern wireless applications.

2.2.7 Tapered Slot Antennas

Tapered slot antenna or Vivaldi antenna engrossed the RF engineers due to its wide impedance bandwidth, narrow beamwidth and small physical width. Prasad and Mahapatra for Microwave Integrated Circuit (MIC) slot line antenna [60] and Gibson for Vivaldi aerial [61] used the modified slot-line antenna structure for endfire radiation. Vivaldi is a non-resonant travelling wave antenna which utilizes a slot-line radiator by extending it in a region where edge separation is greater than the half wavelength. The energy in traveling wave is tightly bound to conductors when the width of the slot is small compared to the free space wavelength. However, when the width is increased, it gradually weakens and eventually radiates at the aperture. If an ideal (no loss) feeding is considered then the lowest operating frequency of Vivaldi antenna can be controlled by aperture opening [61].
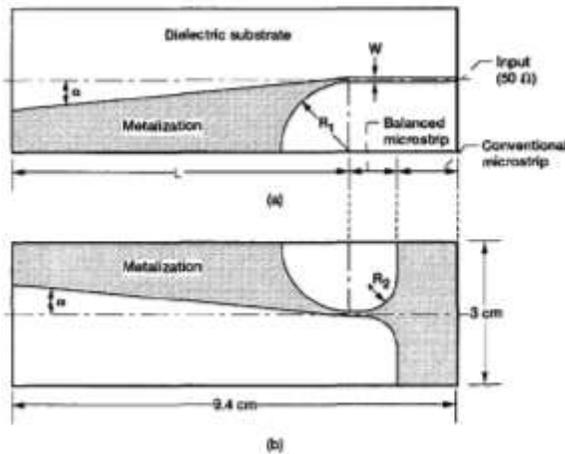
Figure 2.7 Balanced microstrip line fed Tapered slot antenna [62] (a) Top view (b) Bottom view

For an endfire travelling wave antenna, length (L_{ant}) of the antenna has an effect on directivity is typically given by,

$$Directivity \cong m\frac{L_{ant}}{\lambda_0} \qquad\qquad (2.1)$$

where, λ_0 is the free space wavelength. If the length of the antenna is in the range of $3\lambda_0 < L <$ $8\lambda_0$, then m = 10. However, the value of m decreases for antennas longer than $8\lambda_0$ [63].
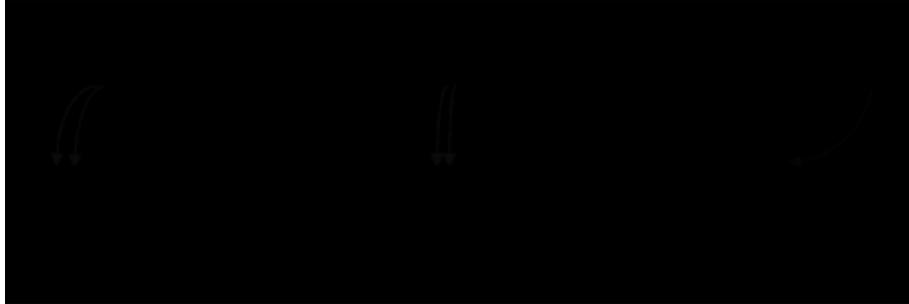
Figure 2.8 Electric field line orientation for (a) unbalanced microstrip line (b) Balanced microstrip line (c) antipodal tapered slot

Numerous ways had been proposed to excite the tapered slot to a design planar structure. Microstrip line is an unbalanced structure due to its ground plane, whereas tapered slot antenna having two conductors separated by a slot, is symmetric or balanced structure. In [62], balanced microstrip is presented to serve the purpose of a balun. Balun (also called as *Bal*ance-*Un*balance) is a transition between balance and unbalanced transmission line which also serves the purpose of impedance matching between the two lines [11]. Ground plane of an unbalanced microstrip line is gradually decreased, as shown in Fig. 2.7, to match the width of microstrip line (W_{50}). Gradual taper facilitates impedance matching between conventional and balanced microstrip. Non-planar tapered slot antenna was designed by flaring the balanced microstrip conductors in the opposite direction. Fig. 2.8 shows the electric field orientation in conventional microstrip, balanced microstrip and non-planar tapered slot antenna. Balanced microstrip has concentrated electric field lines as compared to the unbalanced microstrip line, whereas electric field lines rotate along the axis of the antenna when slot width is increased gradually [62]. Non-planar tapered slot antenna is also called as Antipodal Tapered Slot Antenna (ALTSA).
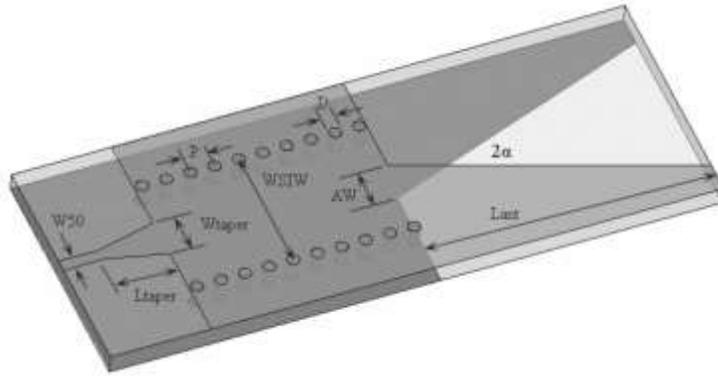
Figure 2.9 SIW fed ALTSA [64]

As substrate integrated waveguide (SIW) is one of the balanced structure having similar electric field orientation as balanced microstrip line, SIW was used for feeding ALTSA. SIW prevails over the conventional microstrip line regarding an insertion loss performance at microwave and MMW frequencies. The typical impedance of ALTSA is approximately 160Ω, whereas impedance of the SIW is limited by the height of substrate. Therefore, tapered slot is backwardly extended to prevent this matching. Low input impedance is obtained by crossing the metallic covers of tapered slot for short distance [64]. Although SIW feed for ALTSA is also proposed in [65], it uses CPW feeding, which is unable to obtain 50Ω input impedance. In [65], minimum input impedance of 74Ω is achieved.

Tapered slot antennas are most suitable for MMW endfire radiation application due to their planar structure, low losses and high gain capability.

2.2.8 Comparison of various Millimeter Wave Antennas

Gain capability and size of structure are few of the important characteristics to achieve the objective of this thesis. Therefore, antenna structures discussed in literature are compared in Table (2.1).

Table 2.1 Gain and size comparison for Millimeter wave Antennas

Antenna Structure	Radiation	Gain capability	Planar structure
Horn Antennas	Endfire	Moderate	Planar/Non-planar
	Broadside	Moderate	Non-Planar
Lens Antenna	Endfire	High	Non-Planar
Dielectric Rod	Endfire	High	Non-Planar
Slot Antenna	Broadside	Moderate	Planar
Dielectric Resonator Antenna	Broadside	Moderate	Non-Planar
Microstrip Antenna	Broadside	Moderate	Planar
	Endfire	Moderate	Planar
Tapered Slot Antenna	Endfire	High	Planar

In a summary, highly efficient dielectric resonator antennas proposed for the broadside radiation. However, they achieve only moderate gain and more importantly offer non-planar structures. Although lens antennas have exhibited the high gain, they have non-planar structure as well. As in planar structures, slot apertures and printed antennas are proposed. However, slot apertures suffer from higher ohmic losses. In case of endfire radiation, although horn antennas are proposed in planar structure, they offer relatively lower gain for the endfire case. Even dielectric rod antennas which are proposed for endfire radiation have non-planar structures.

2.3 Numerical Techniques for Full wave analysis

Radiation fields and scattering matrix of an antenna can be obtained by solving the Maxwell equations satisfying the boundary conditions for the structure. At the core of any electromagnetic problem are the Maxwell's equations. Solution of Maxwell's equation without

any physical approximation is called as Full wave analysis. However, the actual solution of Maxwell's equations is very complex and computational electromagnetics is used to solve the Maxwell's equations using computer programs. There are numerous CAD tools available for full wave analysis of electromagnetic structures. Although these tools do not consider any physical approximation, they solve the equations using different numerical techniques which assume certain numerical approximations. Use of any of the numerical methods involves three steps [66]:

1. Preprocessing, to derive the coefficients in the algebraic equations

2. Solutions of the algebraic equations

3. Interpretation of results

Few numerical techniques used for electromagnetics are [66]:

1. Method of Moment (MoM)

2. Finite Difference Time Domain (FDTD)

3. Finite Element Method (FEM)

4. Finite Integration Technique (FIT)

5. Fast Multipole Method (FMM)

6. Transmission Line Matrix (TLM)

7. Uniform Theory of Diffraction (UTD)

Each technique is suitable for particular types of problems. There is not one sufficient and effective technique for all types of electromagnetics problems. Method of moment uses integral equations and it is suitable for the problem which consist of conductive surfaces only, homogeneous dielectrics only or specific conductor-dielectric shapes only. It does not handle electromagnetically penetrable materials [67]. In FDTD method values of the next time step are

calculated based on values at current and previous time steps. Therefore, this method is not unconditionally stable [67]. FDTD method is efficient for problems with non-isotropic materials. It requires grid with size of smallest dimension in structure, it may run into issues of large computational requirement [68]. In TLM, each node is connected to its adjacent node via a pair of orthogonally connected virtual transmission lines. However, similar to FDTD it has problem of large complexity when huge structures are to be analyzed [68]. UTD approximates electromagnetic wave as the light ray. Therefore, it is accurate only for high frequency calculations [68]. Integral solver FMM uses much lesser points to solve the equation. It needs smaller storage memory, however, it is suitable only for plane wave excitations problems [69].

Full wave analysis of antenna structures presented in this thesis is carried out using CST Microwave studio, which uses the Finite Integration Technique (FIT) and HFSS which uses the Finite Element Method (FEM). These numerical techniques are discussed in following sections.

2.3.1 Finite Element Method

The basic concept of the finite element method is that although the behaviour of the function may be complex when viewed over a large region, a simple approximation may suffice for a small subregion. The total structure is subdivided into smaller finite elements. In three dimensional structures tetrahedron, hexahedron, prism, pyramid shapes are used as finite elements because they can cover the complex structures as well. Fields are calculated at nodes and approximated by interpolation on each element using differential expressions. The field representation is continuous at the edges where elements overlap. The equations to be solved are in terms of an integral type functional such as energy. The total functional is the sum of the integral over each element [66].

Figure 2.10 Subdivision of a region using finite elements

The discretization step can be easy or complex depending upon the curvature and size of the structure. Fig. 2.10 shows a simple rectangle has been subdivided using square elements, however irregular triangles are used to divide the irregular and slightly complex shape. For any three dimensional electromagnetic structure, three independent spatial co-ordinates are required for the discretization of the region. Tetrahedron shaped finite elements are used in HFSS CAD tool as they model even the complex structures accurately.

An approximate functional (ϕ_n) is calculated for element n and quantity is interrelated in all N elements such that it is continuous at boundaries. The approximate solution for the whole region is then sum of all element potentials as given by (2.2).

$$\emptyset(x,y) = \sum_{n=1}^{N} \emptyset_n(x,y) \qquad\qquad (2.2)$$
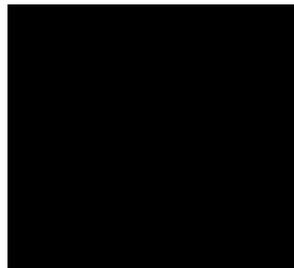
Figure 2.11 Irregular triangular element with three nodes

Functional is generally a polynomial approximation such as (2.3) for triangular element. However, higher order interpolation is required in more complex examples.

$$\emptyset_n(x, y) = a + bx + cy \qquad (2.3)$$

Functional values for vertices of irregular triangular element as in Fig. 2.11 can be given by matrix notation,

$$\begin{bmatrix} \emptyset_1 \\ \emptyset_2 \\ \emptyset_3 \end{bmatrix} = \begin{bmatrix} a \\ b \\ c \end{bmatrix} \begin{bmatrix} 1 & x_1 & y_1 \\ 1 & x_2 & y_2 \\ 1 & x_3 & y_3 \end{bmatrix} \qquad (2.4)$$

The determinant of the coefficients is given by the following equation where A is the area of a triangle.

$$\begin{vmatrix} 1 & x_1 & y_1 \\ 1 & x_2 & y_2 \\ 1 & x_3 & y_3 \end{vmatrix} = 2A \qquad (2.5)$$

When equations are solved for a,b and c. We get,

$$\emptyset(x, y) = \sum_{k=1}^{3} \vartheta_k(x, y)\emptyset_k \qquad (2.6)$$

Which gives,

$$\vartheta_1(x, y) = \frac{1}{2A}[(x_2 y_3 - x_3 y_2) + (y_2 - y_3)x + (x_3 - x_2)y] \qquad (2.7)$$

Similar function is obtained for second and third row. The ϑ_1 are interpolation functions in the sense that,

$$\vartheta_j(x_k, y_k) = \begin{cases} 1 & if\ j = k \\ 0 & if\ j \neq k \end{cases} \qquad (2.8)$$

In case of capacitance example, gradient of $\emptyset(x, y)$ can be used to find the energy in the element. Calculation for two dimensional structure established portrays the complexity to be faced with a huge three dimensional structures.

Error sources in finite element method are discretization, formulation and numerical. Using less number of elements might speed up the process, however it will result in inaccurate results. Shaper of the element can contribute in the error of calculation. Therefore, the proper formulation of specific problem is important. Numerical errors are concerned with the CAD tool program and their ability to handle larger numbers.

2.3.2 Finite Integration Technique

The key concept for the finite integration technique is to use in discretization the integral rather than a differential form of Maxwell's equations. There are two primary aspects of FIT which makes it popular. Firstly, it is not only applicable for frequency domain, but also for time domain calculation. Therefore, huge and complex structures can be solved using FIT. In addition, it is applicable to a variety of discretization types [70].

Prior to start the electromagnetic calculation, the structure is discretized using mesh. Tetrahedron, staircase-hexahedron can be used for it as shown in Fig. 2.12. The hexahedron type mesh is more suitable for time domain calculation, on the other hand tetrahedron type mesh is more suitable for frequency domain calculation and covers the surface with fine details.

If electromagnetic example is considered then Maxwell equations are written for the individual mesh element. For hexahedron element in Fig. 2.12 (c),

$$\overline{e_l} + \overline{e_k} - \overline{e_j} - \overline{e_i} = -\frac{d}{dt}\overline{\overline{b_n}} \qquad (2.9)$$

When all electric and magnetic quantities are considered, Maxwell equation can be written in matrix form.

$$C\bar{e} = -\frac{d}{dt}\overline{\overline{b}} \qquad (2.10)$$
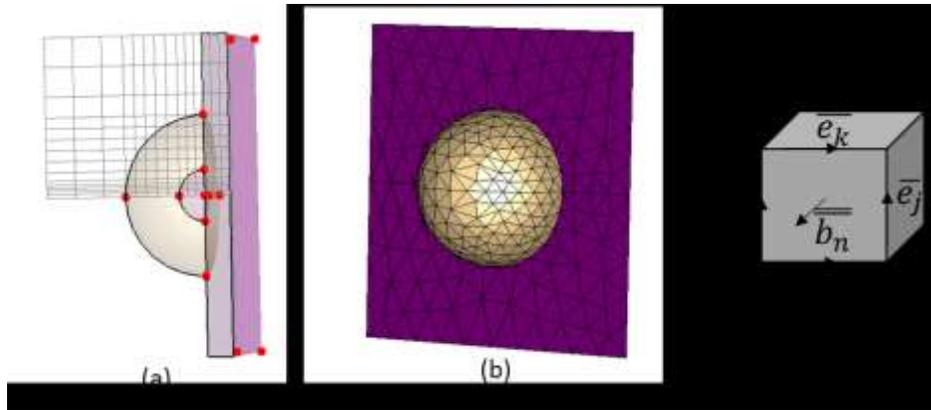
Figure 2.12 (a) Staircase-Hexahedron type meshing (b) Tetrahedron meshing (c) Allocation of voltages and flux on hexahedron element

Here C is a topological curl-matrix and represents edges and faces in an incidence matrix of primary grid. Similarly, equations for $\overline{h}, \overline{\overline{d}}$ and $\overline{j}$ can be obtained from Maxwell's second equation on dual grid. All electromagnetic quantities are transferred to a discrete set of matrices. Solving these discrete Maxwell grid equations allow to obtain all the desired quantities of the structure.

One of the sources of error in FIT algorithm is space discretization error. This is obvious because the solution region can be divided only in a finite number of mesh cells. Method error comes when material properties are discretized for the solution of equations.

2.4 Summary

In this chapter, we have reviewed various millimeter wave antennas including endfire and broadside radiating structures. The discussion covers both planar and non-planar structures, including array antennas to facilitate obtaining higher gain. Furthermore, various full wave analysis methods are reviewed. Two CAD tools, i.e., HFSS and CST, which are based on FEM and FIT algorithms, respectively, are to be utilized for the analysis of two proposed antenna structures. These algorithms are suitable for homogeneous and inhomogeneous material structures at millimeter wave frequencies.

Chapter 3

Four Element Aperture coupled Patch Antenna

Four element aperture coupled patch antenna is presented for Ka-band millimeter wave communication. Section 3.1 introduces microstrip antenna and working of the antenna structure. Section 3.2 elaborates the design methodology for the proposed structure. Section 3.3 shows proposed structure and design parameters. Section 3.4 follows with the study about the effects of various parameters on antenna performance. In the end, section 3.5 exhibits the designed prototype with simulation and measured results.

3.1 Microstrip Antenna

3.1.1 Introduction

General microstrip antenna or Patch antenna structure is shown in Fig. 3.1. It has a thin metal layer suspended by a dielectric medium over a ground plane. Typically, microstrip antenna is broadside radiating structure as its pattern maximum is in the normal direction to the plane of a metal layer [11].
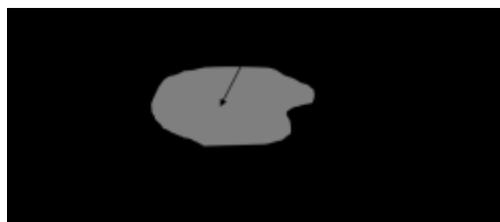
Figure 3.1 Microstrip patch antenna

Linear as well as circular polarization can be achieved by patch antennas. Following characteristics of patch antennas mark them favorable for modern high frequency applications [11]:

1. Planar structure

2. Low profile

3. Compatible with printed circuit technology

4. Easy to use in array structures

3.1.2 Feeding Techniques

Figure 3.2 Various feeding techniques for patch antennas: (a) Coaxial probe feed (b) microstrip line feed (c) Aperture coupled feed (d) Proximity feed

There are four feeding methods used for patch excitation [11]. All of which has their own pros and cons. Microstrip line feed, as shown in Fig 3.2 (b), is easy to fabricate. However, impedance bandwidth using this feed is limited. Although, coaxial feed, as shown in Fig. 3.2 (a), is also easy to fabricate and match with the input impedance, it exhibits narrow impedance bandwidth and not suitable for array designing. The proximity coupling, as shown in Fig. 3.2 (d), uses an open ended microstrip line under the patch within proximity. In this method direct contact of a feed line to a radiating edge is avoided, hence, an improved radiation pattern can be obtained. In aperture coupling, as shown in Fig. 3.2 (c), feed line and patch are on the opposite sides of a ground plane. A slot is cut in the ground plane to couple the energy from one side to another.

Although this method is difficult to fabricate, it provides stronger coupling than proximity feeding. Also, aperture coupling allows high permittivity dielectric material to be used for feed design without compromising low permittivity material in radiation side. Improvement in the impedance bandwidth and compatibility with array design make it favorable for higher gain, wideband applications.

3.2 Design of Four Element Patch Radiator

Fig. 3.3 shows layer structure used for the single patch antenna in this design. Step by step approach for designing or selection of each is explained henceforth.
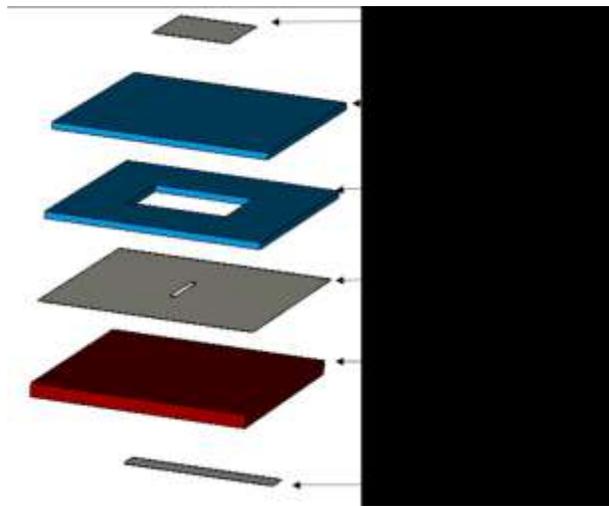
Figure 3.3 Single element aperture couple patch antenna layers

3.2.1 Design of Microstrip line feed

In the proposed structure, an aperture coupling is used to feed the patch. As a slot can be modeled as a dipole, it has bidirectional radiation behaviour. This might result in the high back lobe for patch antenna. Therefore, in order to reduce the back lobe of the structure, high dielectric constant is required for the lower substrate material. RO4350 with dielectric constant (ε_{r2}) of 3.66 is chosen for the structure with standard available height (h) of 0.508mm.

The microstrip line feed is designed for 50Ω. When typical microstrip line, as shown in Fig. 3.4(a), is considered, its electric field lines are shown in Fig. 3.4(b). At the edges, electric field lines are passed partially through the air and partially through the substrate. Due to the non-homogeneous dielectric medium, effective dielectric constant is introduced to account for fringing and the wave propagation in the line. As this effective dielectric constant is the combination of dielectric constant of substrate (ϵ_r) and that of air, its value lies between the range of $1 < \epsilon_{eff} < \epsilon_r$. When w/h ratio is greater than 1, which is generally the case, the value of the effective dielectric constant can be calculated by [71],

$$\epsilon_{eff} = \frac{\epsilon_r+1}{2} + \frac{\epsilon_r-1}{2}\left[1 + 12\frac{h}{w}\right]^{-\frac{1}{2}} \quad\quad (3.1)$$

For a similar case, characteristic impedance (Z_0) of microstrip line is given by [72],

$$Z_0 = \frac{120\pi}{\sqrt{\epsilon_{eff}}\left[\frac{w}{h}+1.393+\frac{2}{3}\ln\left(\frac{w}{h}+1.444\right)\right]} \quad\quad (3.2)$$

Figure 3.4 (a) Microstrip Line (b) electric field line distribution for microstrip line

For $\epsilon_r = \epsilon_{r2} = 3.66$, $Z_0 = 50\ \Omega$ and h = 0.508mm, using (3.1) and (3.2), we get,

$W_{50} = 1.1mm$

3.2.2 Design of Coupling Aperture

In case of an aperture coupling antenna, a slot couples the electromagnetic field from the microstrip line feeding section into the upper side of the ground plane. This slot should be non-

resonant as resonant slot increases the back radiation of the antenna [73]. Length of slot is chosen such that close matching is achieved at the center frequency. It is chosen to fix the resistive part as shown in Fig. 3.6(a). For open transmission line, as shown in Fig. 3.5, voltage is maximum and current is zero at the open end. The distance between consecutive maxima and minima is half a wavelength [74]. First current maximum from open ended line is a quarter wavelength away from the end.

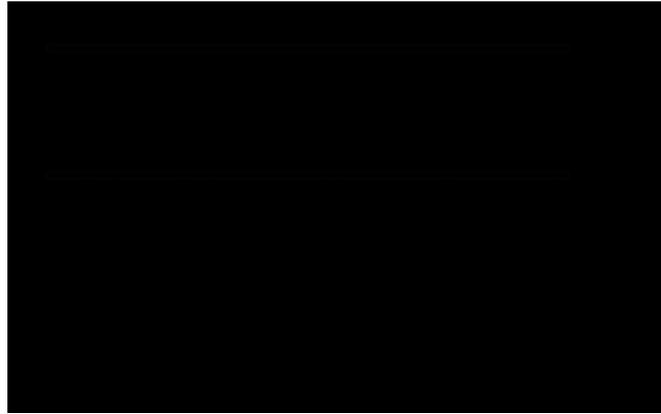

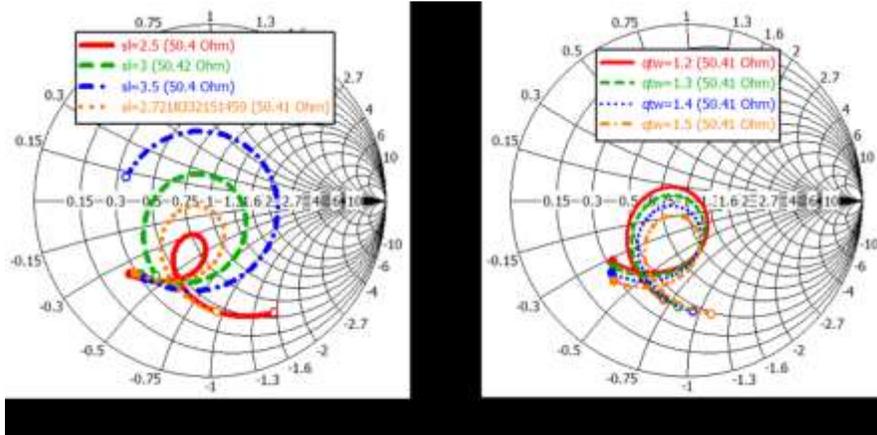Figure 3.5 Open ended transmission line and current distribution over the line

Figure 3.6 Effect on impedance matching of (a) slot length and (b) open stub length

For 28 GHz centre frequency, free space wavelength is $\lambda_0 = \frac{c}{f} = 10.71mm$ and guided wavelength is $\lambda_g = \frac{\lambda_0}{\sqrt{\epsilon_r}} = 5.6mm$. Therefore, theoretically aperture should be positioned

1.4mm away from the open end of the microstrip feed line. However, the length of this open circuit stub has an effect on reactive part of an input impedance of an antenna as shown in Fig. 3.6(b). Therefore, the length of the open stub is chosen to be 1.3mm.

3.2.3 Design of Patch Element

An impedance bandwidth is proportional to the volume of the structure [11]. In case of rectangular patch it can be given by (3.4). Although the length and the width cannot be changed as it will affect the resonance frequency, an impedance bandwidth can be improved by increasing the height of the structure. Nevertheless, if (3.3) is rewritten using electrical dimensions, then (3.4) is relates the impedance bandwidth to the relative permittivity of the substrate. Therefore, the impedance bandwidth of the patch is inversely proportional to the square root of the relative permittivity of the substrate.

$$Bandwidth \sim Volume = length \times width \times height \qquad (3.3)$$

$$Bandwidth \sim \frac{1}{\sqrt{\epsilon_r}} \times \frac{1}{\sqrt{\epsilon_r}} \times \sqrt{\epsilon_r} = \frac{1}{\sqrt{\epsilon_r}} \qquad (3.4)$$

If the air gap of thickness Δ is introduced below the substrate of height 'h' and relative permittivity ϵ_r then equivalent relative permittivity can be given by [73],

$$\epsilon_{req} = \frac{\epsilon_r(h+\Delta)}{(h+\Delta\epsilon_r)} \qquad (3.5)$$

Therefore, air gap of 0.254mm is introduced with substrate RO6002 height (h) of 0.127mm. RO6002 has relative permittivity of 2.94. Using (3.5), equivalent a relative permittivity is 1.15 is obtained. Due to the fringing effect, a patch looks larger than its physical dimensions, as illustrated in Fig. 3.7. Effective length (L_{eff}) is larger by ΔL from both sides.
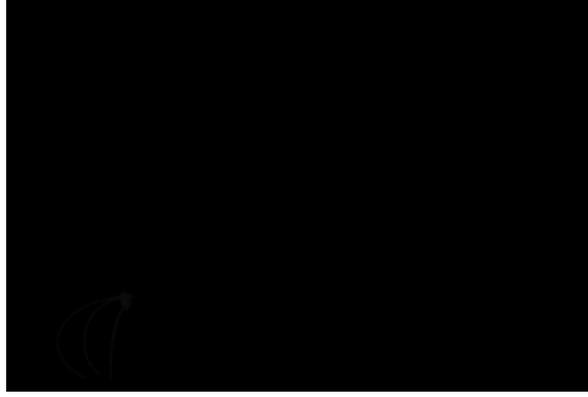
Figure 3.7 Fringing effect in patch antenna (a) Top view (b) side view

The transmission line model is utilized for designing the patch element [11]. For the center frequency of 28 GHz, ε_{req} = 1.19 and h = 0.508mm, we get,

$$W_{patch} = \frac{1}{2f_r\sqrt{\mu_0\epsilon_0}}\sqrt{\frac{2}{\epsilon_{req}+1}} = 5.11mm \qquad (3.6)$$

$$\epsilon_{reff} = \frac{\epsilon_{req}+1}{2} + \frac{\epsilon_{req}-1}{2}\left[1 + \frac{h}{W_{patch}}\right]^{-\frac{1}{2}} = 1.185 \qquad (3.7)$$

$$\Delta L = 0.412h\frac{(\epsilon_{reff}+0.3)\left(\frac{W_{patch}}{h}+0.264\right)}{(\epsilon_{reff}-0.258)\left(\frac{W_{patch}}{h}+0.8\right)} = 0.318mm \qquad (3.8)$$

$$L_{patch} = \frac{1}{2f_r\sqrt{\mu_0\epsilon_0}\sqrt{\epsilon_{reff}}} - 2\Delta L = 4.422mm \qquad (3.9)$$

3.2.4 Improvement of Gain using Multiple Elements

Antenna array is a group of antenna elements positioned and fed strategically to improve the antenna performance. For planar antenna array of N elements, theoretical directivity can be calculated by (3.10) [75].

$$Array\ directivity_{dB} = element\ directivity_{dB} + 3\log_2 N \qquad (3.10)$$

Figure 3.8 Array factor for four elements uniformly fed equidistant array

Fig. 3.8 shows, an array factor for uniformly excited equally spaced four elements. If the distance between successive elements is greater than the critical value, second major lobe will appear in the radiation pattern of an array. This undesirable major lobe is called as a grating lobe. As shown in Fig. 3.8, a grating lobe can be avoided by keeping the value of ψ less than 3π/2. Variable ψ is dependent on the distance between elements which gives an upper bound for distance between elements [75].

$$d < \frac{3\pi}{2} \cdot \frac{\lambda_g}{2\pi} < 0.75\lambda_g < 7.36mm \qquad (3.11)$$

The behaviour of a current on transmission line is already discussed in section 3.2.2. From Fig. 3.5, a maxima reoccurs after every Nλ/2 distance from the first maxima. Therefore, spacing between aperture slots is kept a guided wavelength. It also satisfies the (3.11).

$$spacing = \frac{\lambda_0}{\sqrt{\epsilon_r}} = 5.59mm \qquad (3.12)$$

It completes the theoretical design procedure for patch element.

3.3 Proposed Structure and Design Parameters

Fig. 3.9 shows the proposed antenna structure of four element patch antenna. Dimensions of the structure are 31 x 10 x 0.94 mm^3. Table (3.1) gives the optimized dimensions of design

parameters. Table (3.2) exhibits the details of dielectric materials used for the structure. Results are discussed in the following sections.
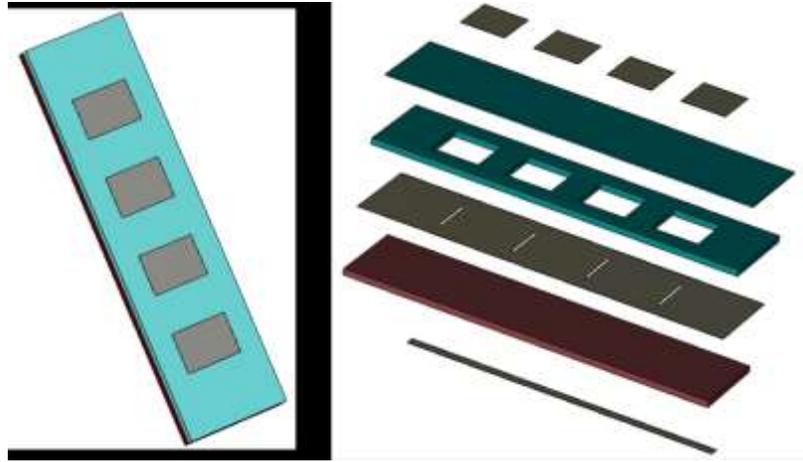
Figure 3.9 Proposed four element patch antenna structure (a) in 3D and (b) in layer separation view

Table 3.1 Design parameters and their dimensions for proposed structure

Design Parameter	Dimension (millimeter)
Length of patch element (L_{Patch})	3.2
Width of patch element (W_{Patch})	5.5
Length of substrate (L)	31
Width of substrate (W)	10
Length of air-gap cavity (L_G)	4
Width of air-gap cavity (W_G)	5.5
Height of air-gap cavity (H_G)	0.254
Height of upper substrate (H_U)	0.127
Distance between elements (Spacing)	6.3
Length of aperture(SL)	5.4
Width of aperture(SW)	0.21
Length of open stub (QTW)	1.29

Table 3.2 Properties of utilized dielectric mediums

Substrate	Dielectric Material	Relative Permittivity	Tangent Loss At 10GHz	Metal Thickness (mm)
Upper Substrate	RO6002	2.94	0.0012	0.017
Lower Substrate	RO4350	3.66	0.004	0.017

3.4 Parametric Study

3.4.1 Lower Dielectric Substrate
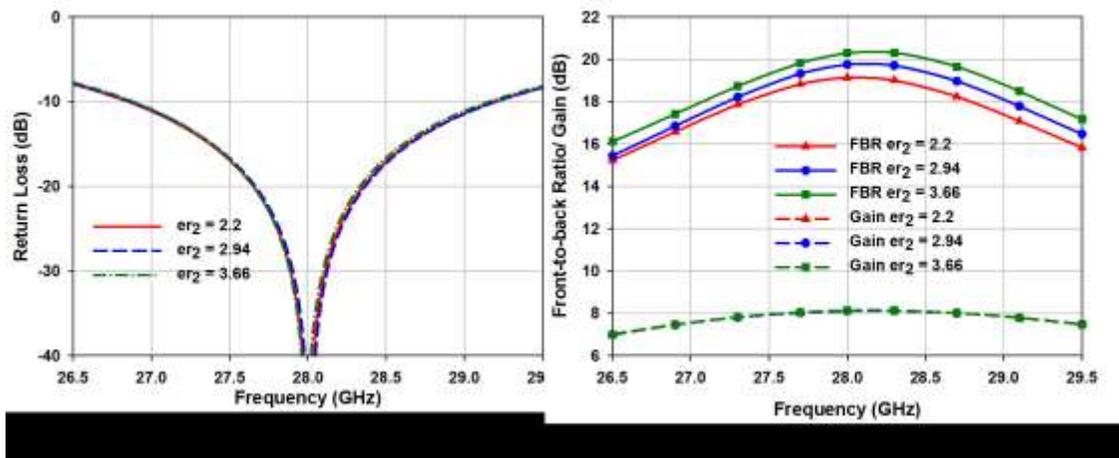
Figure 3.10 Effect of a lower dielectric substrate material on (a) return loss (b) gain and front to back ratio

One of the main advantages of an aperture coupled feeding is that different substrate can be utilized across the ground plane to improve the performance. Changing the dielectric substrate in the lower side of ground plane allows the improvement in a radiation pattern without affecting the characteristics of a structure. Fig. 3.10 shows the effect of different lower dielectric constants on a return loss, gain and front-to-back ratio of the antenna. It can be seen, that there is a negligible effect on return loss and

gain of the structure as a dielectric constant is changed. However, increasing the dielectric constant of a lower substrate improves the front-to-back ratio of the antenna as apparent in Fig. 3.10(b).

3.4.2 Effect of air-cavity

Air-cavity in upper substrate allows the increment in effective electrical size of the structure. The performance of the patch antenna with and without an air gap cavity is illustrated in Fig. 3.11. It is clear from the results that air cavity facilitates to improve the impedance bandwidth of an antenna. In addition, when the air-gap is used, field lines are not held back tightly by the substrate. Therefore, a realized gain of the antenna shows improvement of approximately 1.5 dB for a single element.
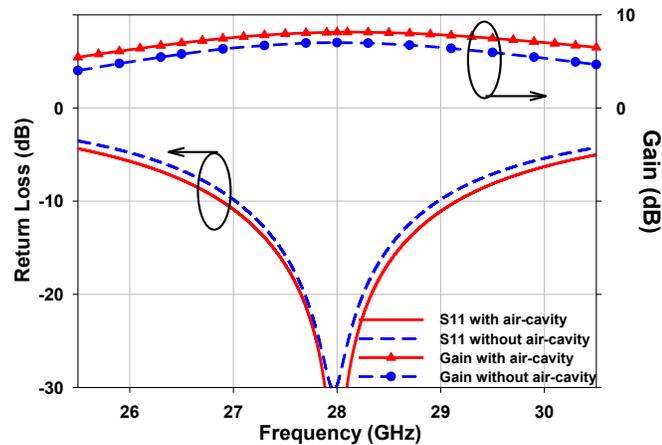
Figure 3.11 Effect of air-gap cavity on a single element patch antenna performance

3.5 Prototype and Results

3.5.1 Single Element Patch Antenna

Fig. 3.12 shows the return loss of single element patch antenna designed in section 3.2. Antenna exhibits an impedance bandwidth of greater than 7.8% with both CST and HFSS simulators. Fig.

3.12 also depicts the gain response of a single element antenna. It has flat again over frequency band at a level of 7.5-8 dB. It can be observed that gain dips down as operating frequency decreases, because the electrical length of the patch is becoming much smaller than half a wavelength.
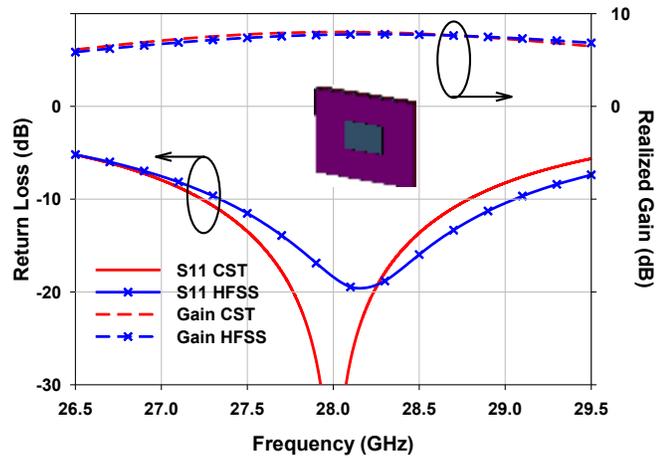
Figure 3.12 Return loss and gain of the single element patch antenna using CST and HFSS
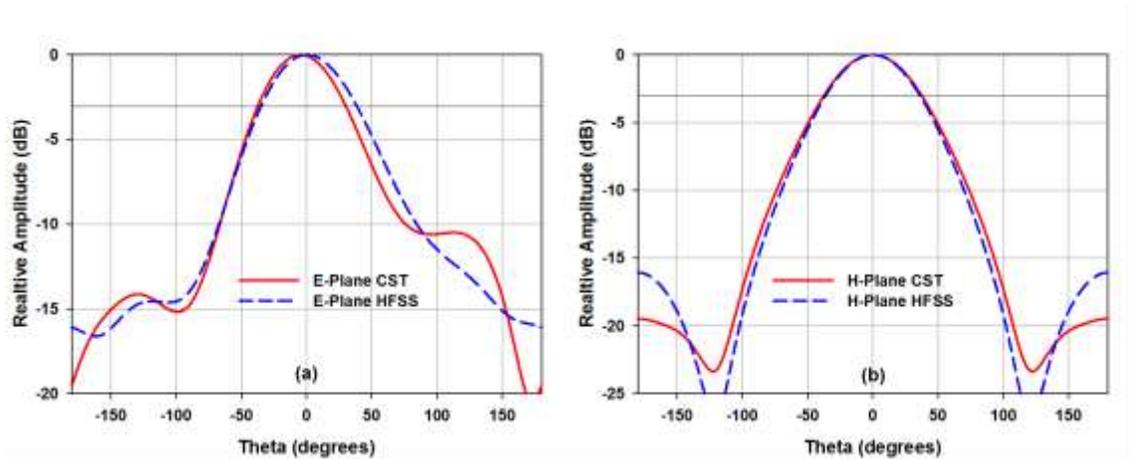
Figure 3.13 (a) E plane and (b) h plane radiation pattern of single element patch

Radiation patterns resulted from the single element patch are shown in Fig. 3.13. Both simulators show agreement in radiation pattern results for the structure. It exhibits the maximum amplitude in the broadside direction. Here, Z-axis is normal to the patch surface and the direction of electric field on patch coincides with y-axis. Therefore, XZ plane is H plane,

whereas YZ plane is E plane. Results show the front-to-back ratio of 16.4 dB. Half power

beamwidth (HPBW) of H plane is 79^0 whereas that of E plane is about 72^0. In addition, side lobe

level in E plane is -10.5 dB, which further improves to -19.5 dB in H plane radiation.

These results confirm that proposed single element patch can be utilized to design four element

patch array in order to achieve the high gain in a broadside direction.

3.5.2 Four Element Patch Antenna

The prototype has been fabricated for the four element patch antenna, as shown in Fig. 3.14.

Multilayer PCB fabrication procedure is utilized to manufacture the antenna structure.

Figure 3.14 Prototype for Four element patch antenna structure

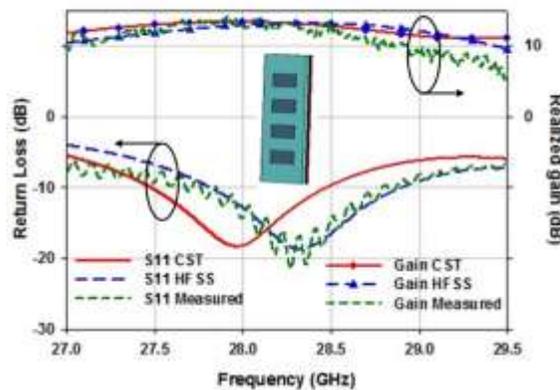

Figure 3.15 Return Loss and gain results for four-element patch antenna from CST, HFSS and measurements

Return loss response for the four-element patch antenna is shown in Fig. 3.15. It can be seen

that antenna exhibits an impedance bandwidth of 1.3 GHz, which is 4.6% of bandwidth at design

frequency of 28 GHz. As discussed before, disagreement between resonance frequency of CST

and HFSS simulators is due to discretization of dielectric material properties. The gain response of the antenna structure is also depicted in Fig. 3.15. A gain of 13.8 dB is achieved at the design frequency. In addition, it exhibits flat gain over the entire frequency band at the level of 13 dB.

Simulation and measurement results are in sync for presented antenna structure. The return loss response of HFSS is more accurate as compared to measured performance. Measured gain response is also in accordance with simulated results. It exhibits the maximum gain of 13.8 dB. Gradual decline in the gain at higher frequencies has been observed. This decline maybe due to mismatch and phase variation across elements at higher frequencies. As series feeding is used to feed the antenna structure, electrical distance between the elements changes as the operating frequency is increased.

The radiation pattern for the proposed antenna structure is presented in Fig. 3.16. Length of the substrate is adjusted such that the maximum amplitude of the radiation pattern is in the direction of the normal to the patch surface. Front-to-back ratio is improved to 24 dB as compared 16 dB for single element. Side lobe levels for the E-plane and H-plane are -14.5 dB and -23 dB respectively. Half power beamwidth of 70^0 is obtained H-plane, whereas that of E-plane is 21.8^0. This reduction in E-plane HPBW is a cost being paid to obtain the higher gain from the structure. As a radiation pattern for an array is a vector multiplication of array factor and element factor, more than one side lobes are obtained. However, proper placement of antenna element has resulted in suppression of these side lobes in E-plane.

Measured results are in accordance with simulated results. It has been seen that main lobe is fairly accurate in both the simulators and SLL of -13 dB and -18 dB are obtained. However, higher back radiation than simulated results has been observed.
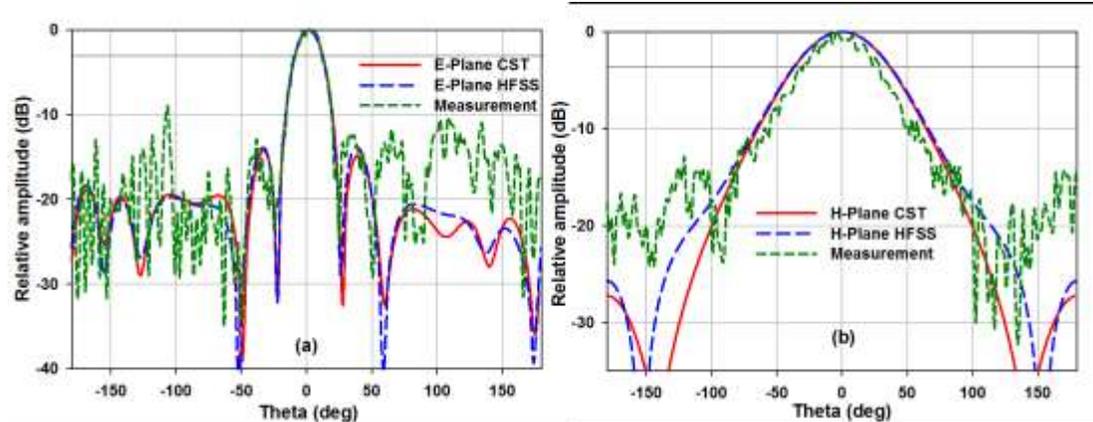
Figure 3.16 (a) E plane and (b) H plane radiation pattern for proposed structure

Fig. 3.17 illustrates the effect of changing the operating frequency on the radiation pattern of the proposed antenna structure. No significant effect was observed in H plane radiation at lower and higher end frequencies. However, as clear from Fig. 3.17 (a), peak of the radiation pattern shifts towards the forward direction as the operating frequency is increased. In addition, side lobe level in the backward direction deteriorates with an increase in the frequency.

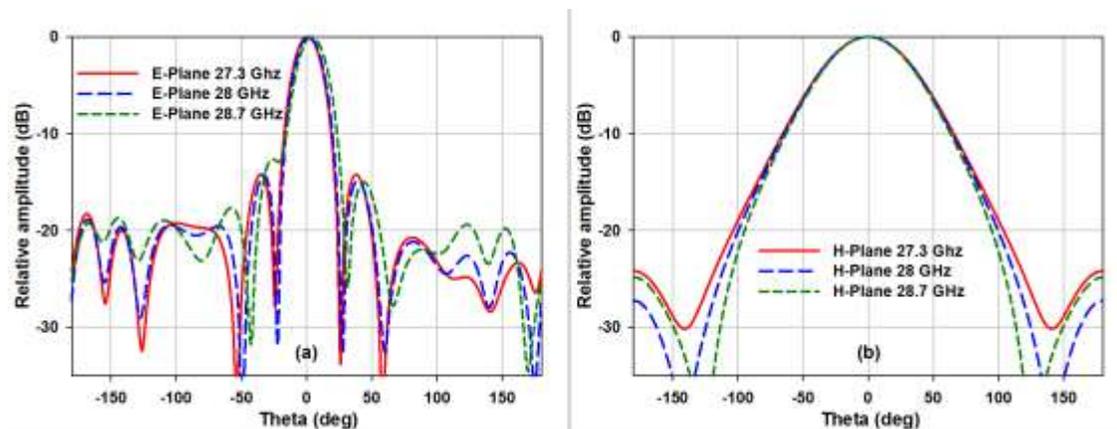*Figure 3.17 (a) E plane and (b) H plane radiation patterns of proposed antenna structure at 27.3, 28 and 28.7 GHz*

Fig. 3.18 shows the efficiency of the antenna structure. Dielectric material, metallic patch as well as microstrip line contribute to ohmic losses in the proposed antenna structure. However, total efficiency above 85-90% is observed in the operating frequency band.
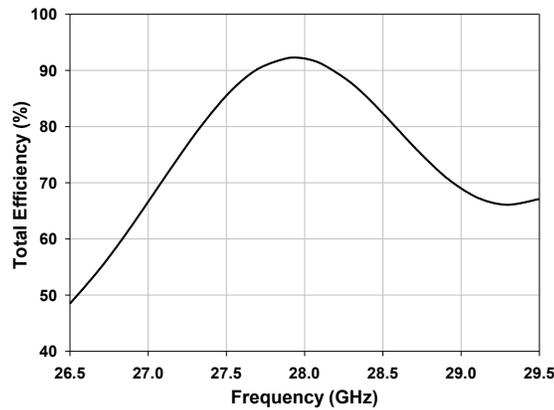
Figure 3.18 Total efficiency of the proposed antenna structure

Table 3.3 Comparison of proposed antenna with broadside radiating antennas in literature

Antenna Structure	Frequency (GHz)	Electrical Size	Gain (dB)
Multilayer Horn [28]	70-105	8.8λ x 5.9λ x .1λ	9.5
Hybrid Horn [25]	28-35	2λ x 1.5λ x 1λ	11
Half Maxwell lens [38]	49-51	5λ x 5λ x 2.3λ	10-20
Circ. Polarized printed [55]	40-48	NA	10
Twin dipole array [57]	29.5-30.5	0.53λ x 0.4λ x 0.22λ	7.7
Vertical patch [59]	50-80	2λ x 2λ x 0.2λ	9
Stacked Patch [58]	26-40	5λ x 3λ x 0.25λ	6
Proposed structure	27.6-28.9	3λ x 1λ x 0.1λ	12.5-13.5

Table (3.3) shows the comparison of a realized gain of numerous millimeter wave antenna structures discussed in the literature for broadside radiation. It can be seen that a proposed structure offers higher gain than most of the structures discussed in the literature. Antennas included here operate at frequencies between 2 to 100 GHz range. Although half Maxwell fish-eye lens antenna offers higher gain than proposed structure, it has large, non-planar structure which limits its applications.

Chapter 4

Antipodal Fermi-Linear Tapered Slot Antenna

The planar antenna structure of Antipodal Fermi-Linear tapered slot antenna (AFLTSA) is presented in this chapter for high gain and wide impedance bandwidth at Ka-band operation. Section 4.1 elaborates the design methodology for AFLTSA. Three design variations of AFLTSA are considered in the analysis. Section 4.2 discusses the effect of various antenna design parameters on the performance of the structure. Fabricated prototypes and measurement setup for the design are presented in section 4.3. Section 4.4 presents the results of simulation and their comparison with measured data.

4.1 Design Methodology

Tapered slot antenna and its radiation principle are discussed in chapter 2. This section specifically concerns about the proposed structure. Fig. 4.1 shows the proposed Antipodal Fermi-Linear Tapered Slot Antenna structure and its design parameters. Structure of AFLTSA can be divided into two main sections, namely, (a) a feeding section and (b) a tapered slot section. Feeding section can be further divided for design purpose in SIW, microstrip and SIW-to-microstrip transition. On the other hand, tapered slot section consists of a tapered slot curve and the corrugation profile at the edges of metallic flare.
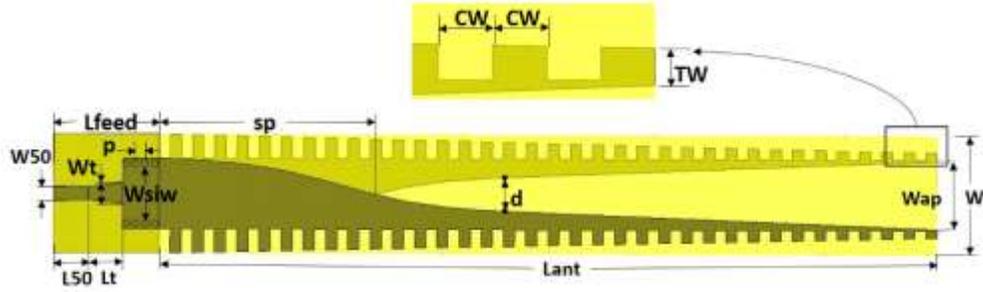
Figure 4.1 Proposed AFLTSA structure with design parameters

4.1.1 Design of feed section

The choice of a dielectric medium for the tapered slot antenna is fairly complicated. A lower dielectric constant will allow the travelling wave to propagate without much blockage. However, it increases the guided wavelength which results into the physically larger structure. On the other hand, higher dielectric constant will allow to design a compact structure. However, it offers certain blocking for travelling wave and reduce the directivity. Therefore, the moderate dielectric constant is chosen to be 2.94. Rogers 6002 dielectric material is used which has tangent delta loss of 0.0012 specified at 10 GHz. For a center frequency of 28 GHz guided wavelength is,

$$\lambda_g = \frac{\lambda_0}{\sqrt{\epsilon_r}} = 6.24mm \qquad (4.1)$$

Various methods to excite the tapered slot are discussed in section 2.2.7. SIW technology is used to reduce the insertion loss and obtain a planar structure. The idea of integrated planar waveguide, later termed as substrate integrated waveguide (SIW), was put forward with the intention of reducing the complex and 3 dimensional bulky transitions between waveguides and planar circuits [76]. The substrate integrated waveguide is fabricated on a single layer of substrate. Metallic layers on top and bottom of dielectric material act as horizontal sides of waveguide, whereas a pair of periodically deployed vias or metallic posts act as side walls of the

waveguide, as illustrated in Fig. 4.2. The diameter of the vias (D) and the center to center distance between successive vias (p), also termed as pitch, are critical design parameters for substrate integrated waveguide. Pitch should be as small as possible to reduce the leakage through side walls [77]. Following two criteria ensure that there is no radiation loss from side walls of SIW,

$$D < \frac{\lambda_g}{5} < 1.248mm = 0.5mm \qquad (4.2)$$

$$p \leq 2D < 1mm = 0.86mm \qquad (4.3)$$
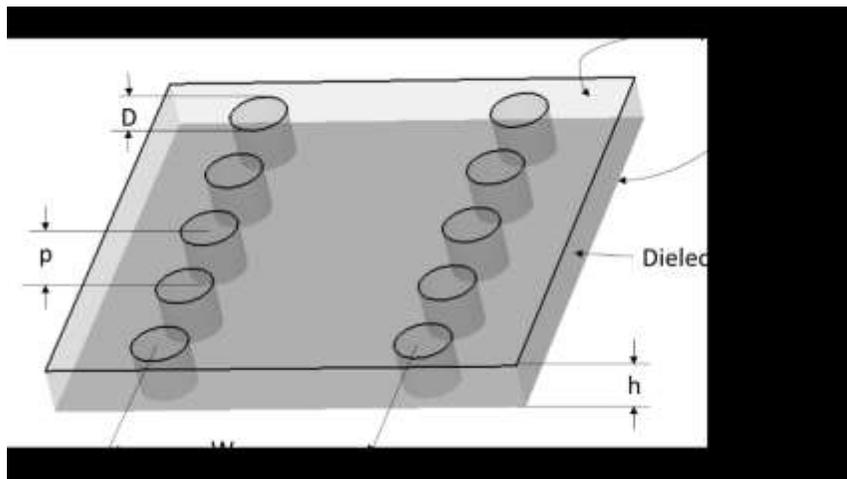
Figure 4.2 Substrate integrated waveguide design

The cut-off frequency is dependent on effective width of SIW (W_{eff}) and effective relative permittivity (ε_r) of the dielectric material as discussed in [78] by following formula,

$$f_{cut-off} = \frac{c}{2W_{eff}\sqrt{\varepsilon_r}} \qquad (4.4)$$

If W_{siw}, as shown in Fig. 4.2, is the physical width of SIW, then W_{eff} of the SIW is between ($W_{siw} - D$) and W_{siw}. For higher values of diameter (D), W_{eff} is dependent on physical width of SIW (W_{siw}), pitch (p) and diameter (D) of vias by following relation [79],

$$W_{eff} = W_{siw} + 1.08\frac{D^2}{p} + 0.1\frac{D^2}{W_{siw}} \qquad (4.5)$$

Putting worst case scenario of (4.3) gives design equation for SIW [78],

$$W_{siw} = 0.5\left[W_{eff} + \sqrt{\left(W_{eff} + 0.54D\right)^2 - 0.4D^2}\right] + 0.27D \qquad (4.6)$$

In the feeding section, SIW physical width should be greater than the minimum width required for the cut-off frequency signal to pass, therefore solving the design (4.6), we get,

$$W_{siw} \geq 3.38mm \qquad (4.7)$$

Therefore, W_{siw} is chosen higher than cut-off which also helps increase the coupling.

Figure 4.3 Orientation of Electric field lines in (a) rectangular waveguide and (b) microstrip line

One of the important thing is to have a structure which is easy to combine with other standard circuitry. Therefore, input impedance of 50Ω is required for the antenna. Microstrip line is designed with 50Ω input impedance for specified dielectric material using (3.1) and (3.2) as previously designed for a patch structure presented in chapter 3.

$$W_{50} = 1.2mm \qquad (4.8)$$

As the orientation of quasi transverse electromagnetic (QTEM) mode electric field lines in a microstrip line and that of a TE_{10} mode of the SIW, as shown in Fig. 4.3, are approximately in the same direction a microstrip line is most suitable feed for the SIW.

As the electric field orientation of SIW and microstrip line are similar, the transition between them is fairly simple. Length and width of the tapered microstrip-to-SIW transition is deciding factor for its performance. They are suitably chosen for the better matching and return loss performance. Fig. 4.5 shows quarter wavelength transition is sufficient to match the lines. In addition, Wt shows improvement in performance until a certain limit of width (Wt = 2 mm), after which performance is similar.

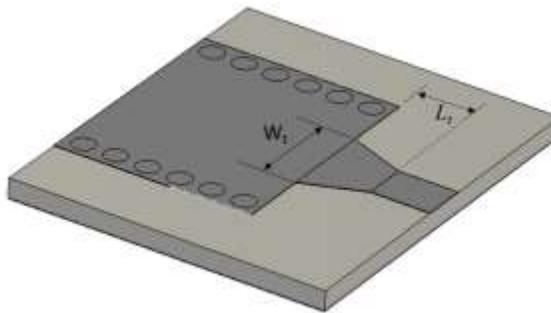*Figure 4.4 Tapered microstrip to SIW transition with design parameters*

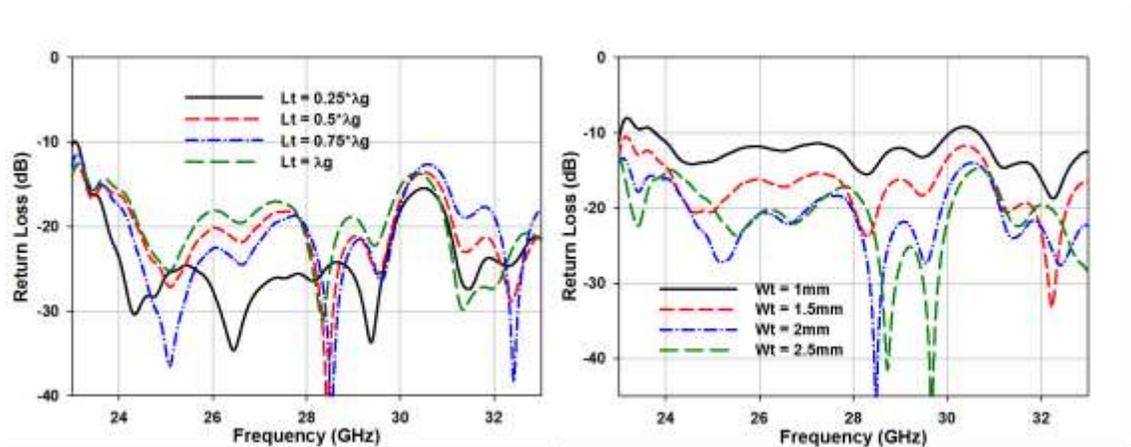*Figure 4.5 Return loss study for microstrip-to-SIW transition design parameters Lt and Wt*

4.1.2 Design of Tapered Slot with Corrugated Edges

In addition, a shape of the taper has a significant effect on the radiation pattern of the TSA. In MIC slot design, as shown in Fig. 4.6(b), slot line was flared linearly [60] whereas in Gibson

design [61], as shown in Fig. 4.6(a), narrow slot was flared towards aperture using following exponential equation:

$$y = \pm 0.125\, e^{0.052x} \qquad (4.9)$$

Figure 4.6 (a) Vivaldi (b) Linear (c) Fermi shaped Tapered Slot Antenna

While LTSA has a narrower beamwidth than Vivaldi, it has higher side lobe levels than Vivaldi [61]. In order to improve the side lobe levels in H plane of TSA, Sugawara et el. introduced Fermi Tapered Slot Antenna (FTSA) [80], as shown in Fig. 4.6(c). In FTSA, the taper of the slot follows the following curve:

$$y = \frac{a}{1+ e^{bx+c}} \qquad (4.10)$$

in this equation, a, b and c are constants which decide the slope, length and width of the curve.

In proposed structure, tapered slot is divided in two parts fermi curve and linear extension. The maximum part of electric field present in SIW should be coupled into the tapered slot. Therefore, fermi distribution of the curve is utilized in the initial part of the tapered slot. Fermi distribution follows (4.10). Shape of this curve serve the important function in this structure as it increases the coupling between SIW and tapered slot.

In order to, generate the radiation from TSA, its aperture width W_{ap} should be greater than half a wavelength at the lowest cut-off frequency. However, if the fermi distribution curve is

continued further along, width of slot increases with the extremely gradual rate. Therefore, fermi distributed curve will require a longer antenna to meet the W_{ap} criterion.

Hence, Fermi distributed curve is followed by a linear curve. This facilitates wider aperture for radiation with relative smaller antenna. Length of an antenna is $\sim 7\lambda_0$.
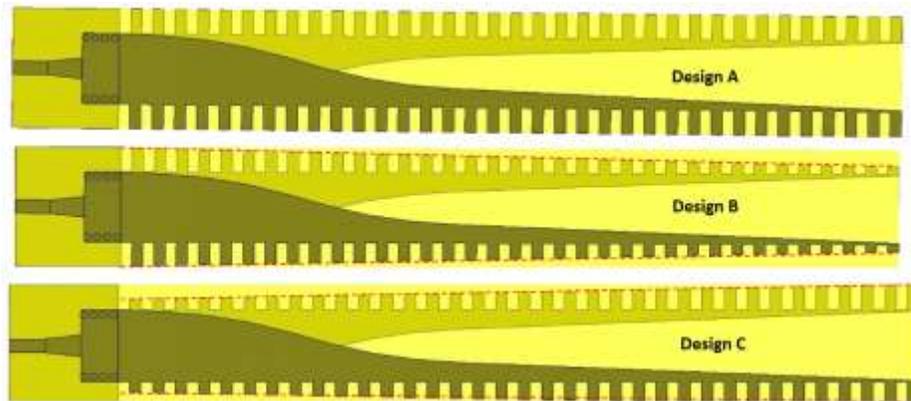
Figure 4.7 Design A, B and C of AFLTSA with different corrugation profile

Due to its endfire radiation and planar structure, TSA is excellent candidate for an array design. However, according to array theory, the distance between consecutive element should be less than λ_0 [75]. TSA having a total width of $2\lambda_0$ shows degraded radiation pattern [80]. Hence, rectangular or sin corrugation can be used which consist periodically arranged slits in sides of TSA [80][81].

In order to reduce the side lobe level in both planes, corrugations are employed at the edge of the metallic flare [80]. Width of the corrugation is kept as 1mm with 1mm spacing between consecutive slits. Three designs with different corrugation profile are studied, as shown in Fig. 4.7. Design A has uniform corrugation where depth of all slits is equal. Design B has a knife-edge corrugation profile, where depth of the slits is decreasing gradually. In the end design C presents a non uniform corrugation profile with increasing depth of the slits.

4.2 Parametric Analysis

Numerous design parameters of AFLTSA affect the performance of the antenna in terms of matching or radiation pattern or both. Few of the critical parameters are analyzed in this section. This analysis helps in designing the optimum antenna structure for best performance. Parametric study is performed with a full wave simulator of CST Microwave studio.

4.2.1 Distance between SIW and Slot Opening
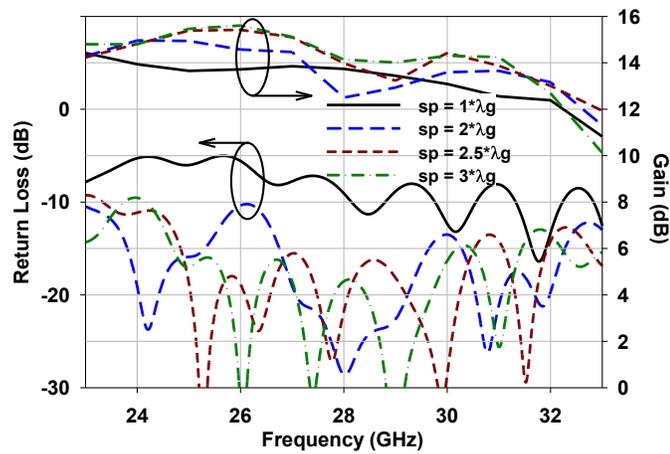
Figure 4.8 Effect of sp on return loss and gain of AFLTSA

Radiating slot begins at the point where top and bottom metallic flares cross each other. The distance between this point and SIW feeding, denoted by 'sp' in Fig. 4.1, has a critical effect on the antenna performance. This distance can be controlled by varying the constants a, b and c of (4.10). This parameter should be kept as small as possible to reduce the overall length of the AFLTSA structure. The effect of this separation distance on the gain and return loss of the antenna is illustrated in Fig. 4.8. For very short distance, there is no coupling between SIW and slot, hence most of the power comes back to an input port. As the distance increases the return loss performance is improved and a wide impedance bandwidth can be achieved. Similarly, the gain of the antenna improves with an increase in the distance, the reason being a smoother

transition between SIW and slot. Therefore, this distance is chosen to be sufficient for coupling and small enough for reducing the length of an AFLTSA.

4.2.2 Separation between End Points of Fermi Curve

The separation between the end points of fermi curve, denoted by 'd' in Fig. 4.1, basically controls the opening of a tapered slot. The effect of this distance on the gain of the AFLTSA is shown in Fig. 4.9. It can be seen that as slot opening increases the gain of the antenna increases linearly. However, as the width of the antenna is limited, we cannot increase this distance beyond a certain limit. Therefore, this distance is chosen to be optimum for easy design and maximum gain.
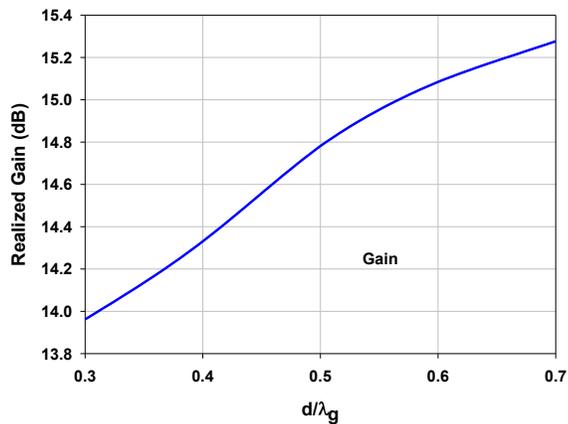
Figure 4.9 Effect of d on realized gain of the AFLTSA

4.2.3 Width of Corrugation

It has been presented in literature that corrugation alongside the tapered slot improve the side lobe levels in the radiation pattern. Generally, extremely narrow corrugations are employed at the edge of TSA [65][80]. Fig. 4.10 shows the effect of corrugation width on the side lobe level in both planes. It can be seen that having corrugation width greater than $\sim 0.16 \lambda_g$ deteriorates the side lobe level rapidly. However, the lesser corrugation width does not have a large effect.

Therefore, corrugation width can be chosen to satisfy the low side lobe level performance and ease in the fabrication process.
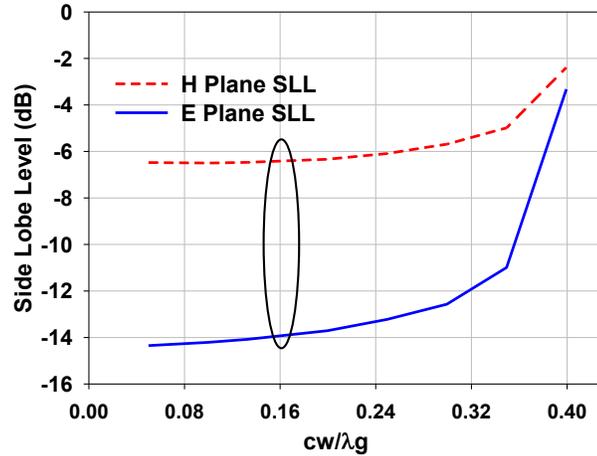
Figure 4.10 Effect of corrugation width on E and H plane side lobe level

4.2.4 Blending the Corrugated Edges
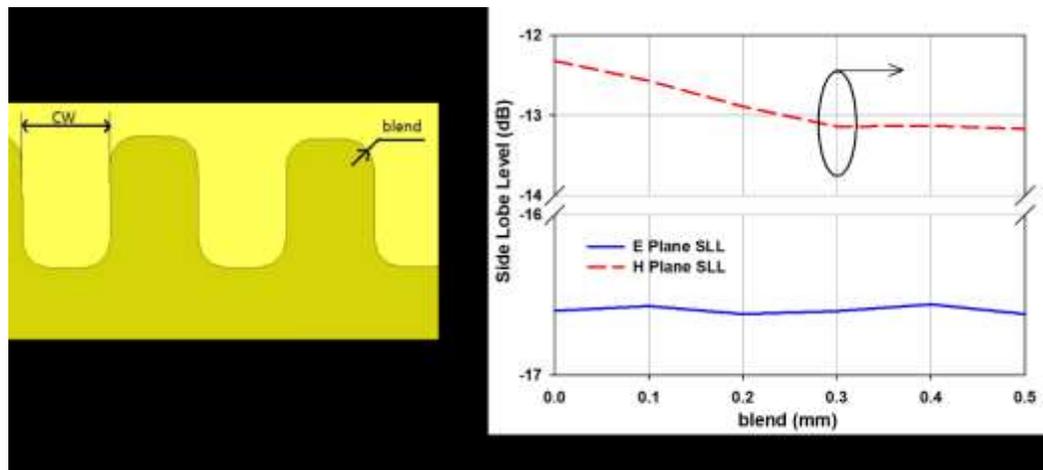
Figure 4.11 (a) blended corrugations and (b) effect of corrugation on side lobe levels of the AFLTSA

At millimeter wave frequencies, sharp edges have an adverse effect on antenna radiation behavior as the operating wavelength gets smaller. To study the effect of sharp edges, blending is applied to the sharp edges of corrugation. Fig. 4.11(a) shows the zoomed view of corrugation with blended edges. In Fig. 4.11(b), an effect of

blending can be seen on a side lobe level in E and H planes. E plane side lobe level improvement of 1 dB is observed with blending of 0.3mm. However, no effect was observed on H plane side lobe level performance due to the blending of edges. In addition, for blending of more than 0.3 mm, there is no improvement as sharp edges are already vanished.

4.3 Prototypes and Measurement Setup

Various antenna parameters and optimized dimensions of the same are given Table (4.1).

Table 4.1 Design parameters and dimensions of AFLTSA

Design Parameter	Dimension in millimeters
Length of Antenna (L_{ant})	74
Length of feed (L_{feed})	9.5
Width of AFLTSA (W)	10.25
Width of corrugation (W_f)	1
Width of SIW (W_{SIW})	5.4
Width of aperture	6.2
Width of microstrip	1.2
Diameter of via	0.5
Pitch of SIW	0.86

AFLTSA structure prototypes, shown in Fig. 4.12, for all three designs of corrugation profile are fabricated using printed circuit board technology. Rogers 6002 dielectric material is used with

0.017mm of copper layers on either side. RO6002 has effective relative permittivity of 2.94. Total size of the structure is 83.5 x 10.25 x 0.508 mm^3.

Figure 4.12 Top and bottom views of (a) Design A, (b) Design B and (c) Design C
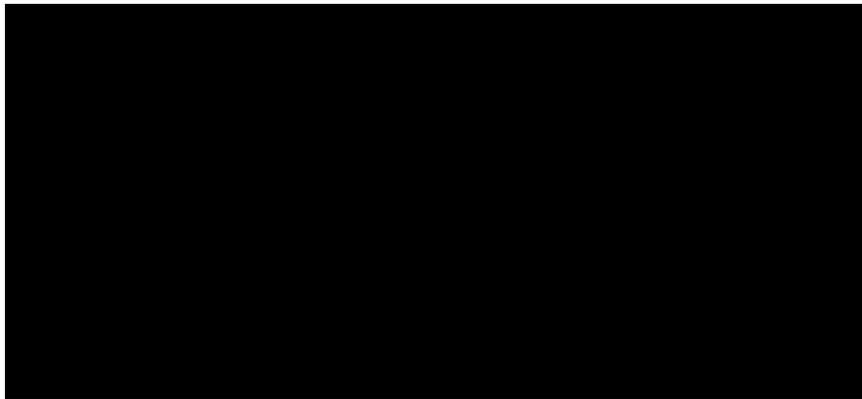
Figure 4.13 Schematic for radiation pattern and gain measurement setup

Return loss measurement is performed using Agilent E8364B vector network analyzer. Measurement of radiation patterns is carried out inside the anechoic chamber as shown in Fig. 4.14 (a). The system is equipped with MI technology compact range system for antenna measurement. Schematic of measurement setup inside the chamber is shown in Fig. 4.13.

Standard transmitter antenna for Ka-band is used to illuminate the reflector in the chamber. Then the test antenna is utilized to receive the power from the reflector. Automatic rotation system is used to measure the power in all angles of theta as well as both E-H planes.
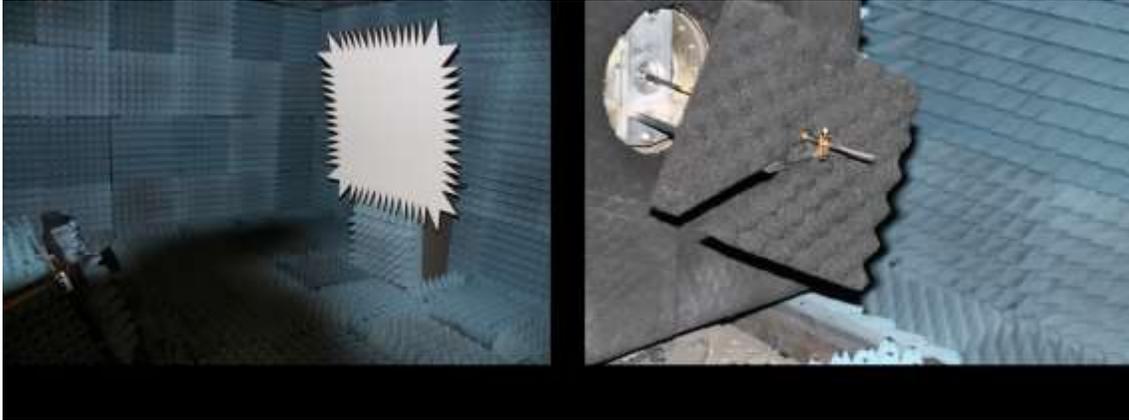
Figure 4.14 (a) anechoic chamber having measurement setup (b) antenna under test

4.4 Result and Discussion

AFLTSA structure is simulated with CST Microwave studio and HFSS. Simulation and measurement results of the proposed structure are compared and discussed in this section. It can be seen that good agreement is obtained between simulated and measured results.
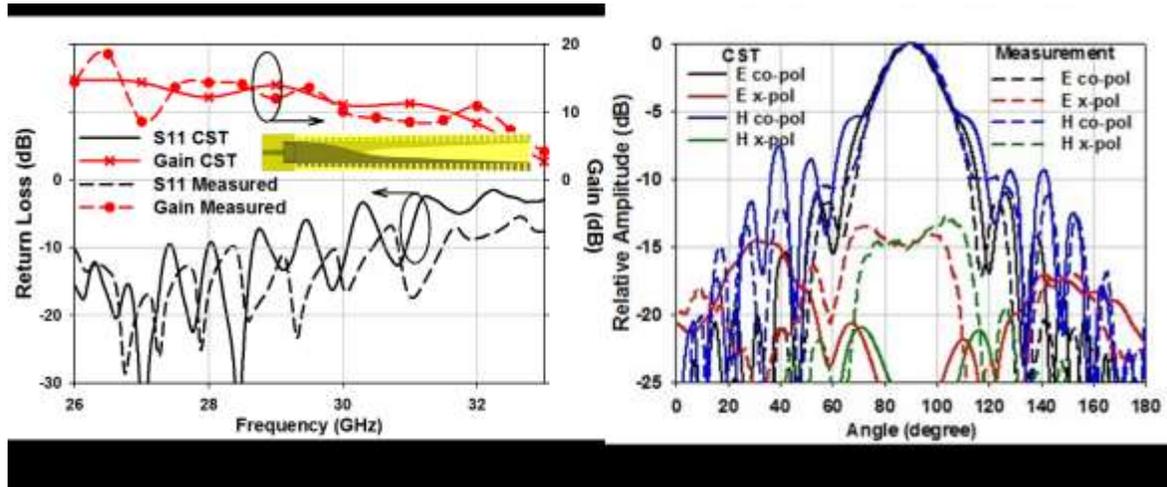
Figure 4.15 (a) Return loss and gain response of Design C (b) E and H plane radiation pattern of Design C at 28 GHz

Design C exhibits higher return loss at higher frequencies, as shown in Fig. 4.15(a). Similarly, its performance degrades at higher frequencies as gain drops below 5 dB level. This has been resulted due to leakage of an electric field from the edges of a tapered slot region where the depth of corrugation is not enough. An electric field distribution in 2D plane cut of Design C, shown in Fig. 4.16, demonstrates the leakage through edges.
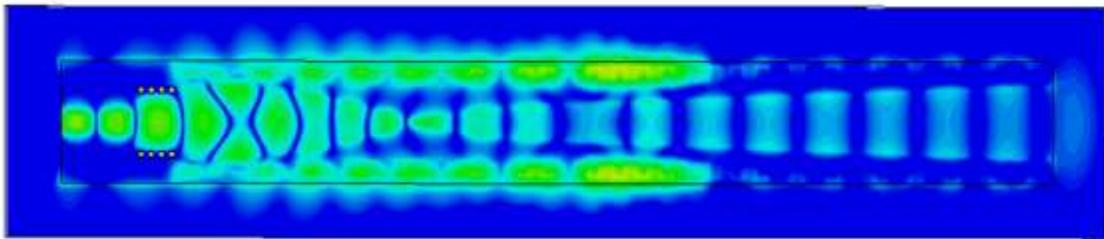
Figure 4.16 2D plane cut view of the Design C showing an electric field distribution

Radiation pattern for Design C, given by Fig. 4.15(b), shows the symmetric radiation pattern until -5 dB level. Design C exhibits E plane side lobe level of -7.8 dB whereas that of H plane is -6 dB. Cross-polarization level for design C is measured to be around -13 dB.
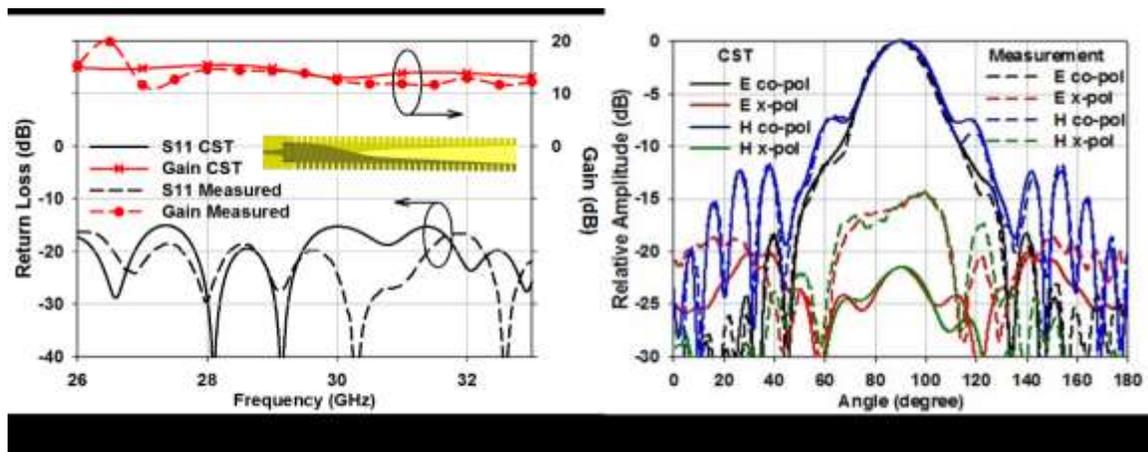
Figure 4.17 (a) Return loss and gain response of Design A (b) E and H plane radiation pattern of Design A at 28 GHz

Design A has much better matching performance than Design C. It exhibits the wide impedance bandwidth, illustrated in Fig. 4.17(a), having return loss level of -15 dB or below. It has flat gain over the entire frequency band at 15 dB level. Radiation pattern in Fig. 4.17(b) for Design A,

shows the symmetric radiation pattern until -7 dB. In addition, side lobe levels in E and H plane are -16.3 dB and -7.4 dB respectively. The cross polarization level for the Design A is quite similar to the Design C at -15 dB level.
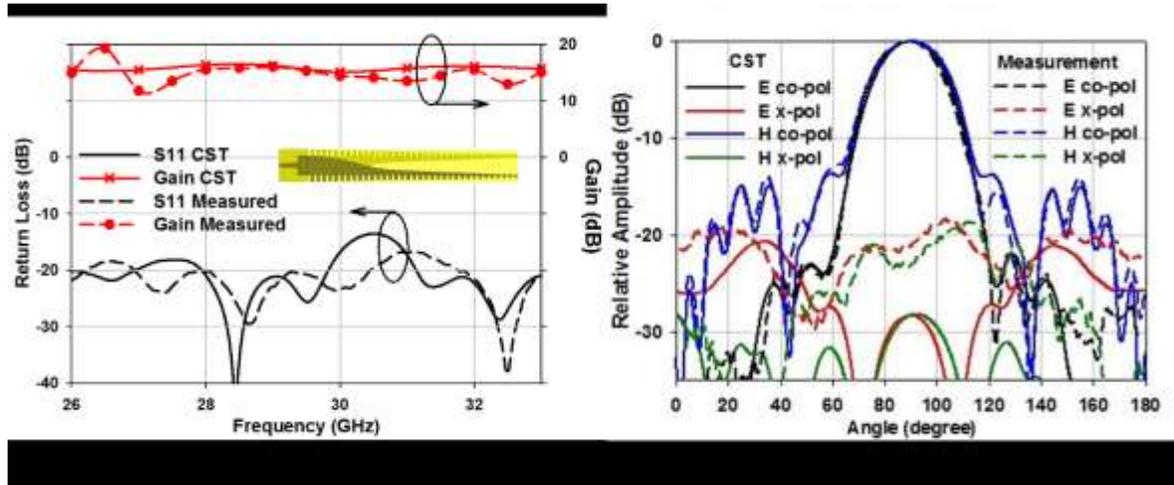
Figure 4.18 (a) Return loss and gain response of Design B (b) E and H plane radiation pattern of Design B
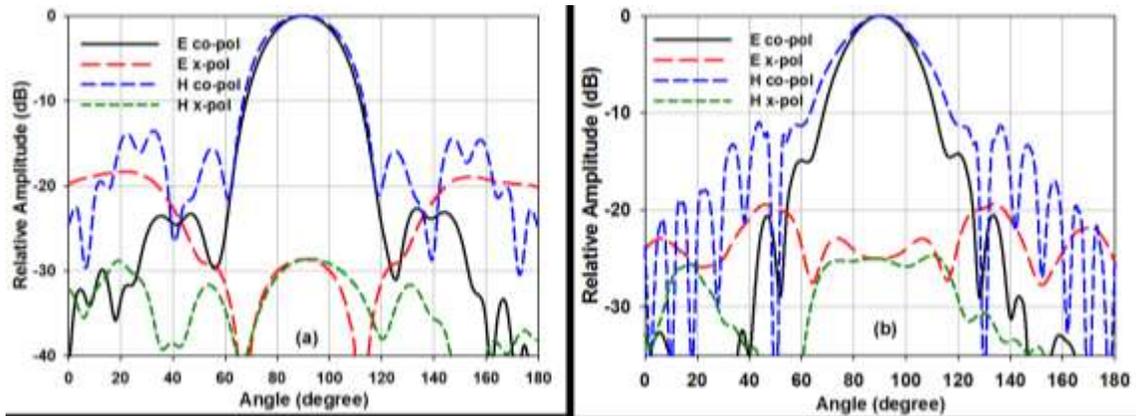
Figure 4.19 Radiation patterns of proposed AFLTSA design B structure at (a) 26 GHz and (b) 33 GHz

Fig. 4.18(a) shows the return loss performance of the Design B which illustrates the wide impedance bandwidth with return loss level below -15 dB. Design B also exhibits the flat gain over the entire frequency band. However, the level of flat gain is higher than that of Design A. It exhibits the gain of 16.4 dB at center frequency of 28 GHz. Radiation pattern in Fig. 4.18(b) shows symmetry in radiation pattern until -13 dB. The measured cross polarization level for the

- 60 -

Design B is improved to -22 dB in both measured planes. Design B has an improved side lobe level of -19.5 dB in E plane and -13.9 dB in H plane.

Fig. 4.19 shows the radiation pattern of design B at lower and higher end frequencies. There is no significant effect on the radiation characteristics of the AFLTSA was observed for lower frequencies. However, at higher frequencies, half power beam width in H plane increases, hence, symmetry in radiation pattern is not maintained. In addition, side lobe levels of both E and H plane are increasing at higher frequency.
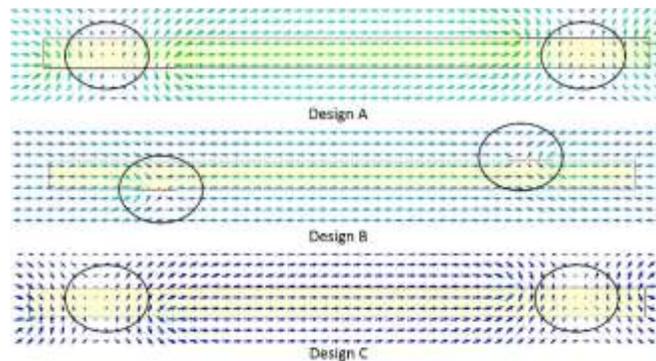
Figure 4.20 Electric field distribution at aperture of the AFLTSA design A, B and C

To understand the difference in radiation performance of these designs, electric field distribution at the aperture, shown in Fig. 4.20, should be considered in detail. Typically an electric field inside the substrate at the aperture of a tapered slot antenna should be in horizontal direction. However, in a region where the substrate is covered with metal, the electric field tends to be vertical. This introduces impurity in an ideal behavior of the electric field. Design A and Design C have metallic corrugation with high depth at the aperture whereas Design B has small depth metallic corrugation at the aperture. Therefore, Design A and Design C show a large disturbance in electric field at places marked by circles. The electric field is almost vertical at these places. On the other hand, Design B has a knife edge model which results in an

undisturbed electric field. Design B exhibits complete horizontal electric field distribution at the

aperture of the AFLTSA.
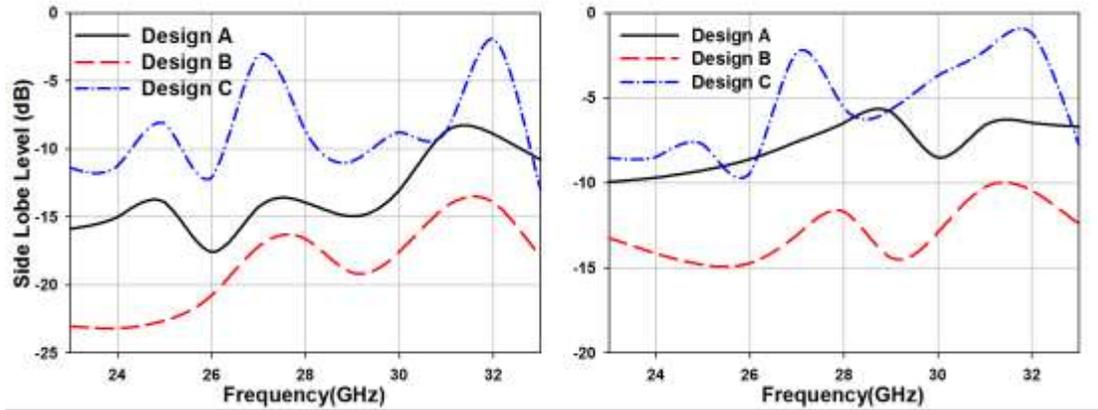
Figure 4.21 E and H plane side lobe level difference for the AFLTSA design A, B and C

This pure electric field helps Design B to focus the radiation pattern in front direction, increase

the gain and reduce the side lobe levels in both planes. The effect of corrugation profile on E

and H plane side lobe levels is presented in Fig. 4.21. Design B exhibits the superior performance

as compared both other counterparts over the entire frequency band.
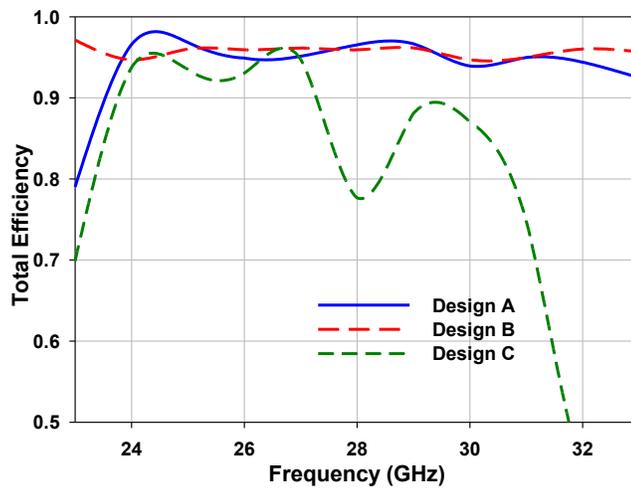
Figure 4.22 Comparison of total efficiency of AFTSA designs

Fig 4.22 illustrates the comparison of total efficiency among AFLTSA structures. Design C has an

unstable performance with a lot of leakage resulting in diminishing efficiency. Design A has good

efficient response except at lower frequencies where its efficiency drops drastically. However, Design B has stable and efficient performance throughout the frequency of operation. It exhibits the total efficiency of 95%.

Table 4.2 Comparison of proposed AFLTSA structure with endfire radiating antennas in literature

Antenna Structure	Frequency (GHz)	Electrical Size	Gain (dB)
Luneberg Lens [38]	29-32	13λ x 12λ x 0.5λ	15-16
CPW fed horn [30]	56-63	5λ x 4λ x 0.4λ	14.2
Coax fed SIW horn [32]	27-28	2λ x 1λ x 0.25λ	5.88
WG fed planar horn [31]	84	9λ x 1.5λ x 0.03λ	9
PTFE SIW horn [33]	22-29	3.2λ x 1.8λ x 0.32λ	8
SIW + horn + TSA [35]	80	3λ x 2λ x 0.15λ	14
Diel. Loaded SIW horn [28]	26-27	3λ x 1.5λ x 0.25λ	12
Hemisphere lens [39]	57-65	NA	21
Linear taper diel. Rod [43]	81	40λ x 4λ x 0.1λ	18.4
Step taper diel. Rod [41]	80-90	4λ x 0.4λ x 0.2λ	13
CPW+SIW+ALTSA [64]	21-31	9λ x 1λ x 0.015λ	15
Proposed AFLTSA structure	25-33	8λ x 1λ x 0.015λ	15.5-16.4

Table (4.2) shows the comparison of a realized gain of numerous millimeter wave antenna structures discussed in the literature for endfire radiation. It can be seen that a proposed structure offers higher gain than most of the structures discussed in the literature. Antennas included here operate at frequencies between 5 to 90 GHz range. Although hemisphere shaped lens antenna and linearly tapered dielectric rod antenna offer higher gain than the proposed structure, they have non-planar structure which limits its applications and deviates from our objective.

Chapter 5

Conclusion

5.1 Conclusion

Ka band (26.5-40 GHz) of MMW frequency is utilized for antenna structure designs. High gain antenna structures are presented to compensate for atmospheric attenuation at Ka band. Printed circuit board technology is used to fabricate two antenna structures. Theoretical design is carried out which is followed by EM simulations to optimize the antenna structure dimensions. Prototypes are fabricated and measurements are performed in anechoic chambers to verify the performance of the designed structures.

Four-element patch antenna is presented for Ka band. The proposed structure exhibits high gain of 13.8 dB in broadside direction. An implementation of the air-gap cavity allows it to achieve the impedance bandwidth of 4.6%. It uses aperture coupling to excite the patch elements which allows a front to back ratio of 26 dB. The wide beamwidth in the H plane of 70^0 can be used for broadcast applications. The proposed structure exhibits a side lobe level of -14.5 dB and -23 dB in E and H plane, respectively. This structure exhibits the efficiency above 85% in operating frequency band.

Antipodal fermi linear tapered slot antenna (AFLTSA) is presented for endifire radiation at Ka band. Proposed structure achieved a flat gain of 16 dB over the entire operating band. Substrate integrated waveguide technology to feed the tapered slot allows the improvement in return loss and matching. Furthermore, simple microstrip to substrate integrated waveguide transition ensures the input impedance of 50Ω can be achieved. It exhibits a wide impedance bandwidth

of 10 GHz in measurement with a return loss level below 15 dB. The proposed structure exhibits a symmetric radiation pattern till -13 dB level. It has lower side lobe levels of -13.9 dB and -19.5 dB in H and E plane respectively. It also exhibits low cross polarization level of -22 dB. This efficient antenna structure exhibits the efficiency of 95 % throughout the operating frequency band. PCB fabrication process makes the design a low cost structure.

5.2 Contribution

Millimeter wave communication has a major role to play in upcoming decades of wireless communication. Most of the demands of wireless application users can be satisfied by the millimeter wave communication. This thesis has the following contributions to the millimeter wave antenna designing field.

1. The designed and fabricated four element patch antenna array [82] achieved a higher gain (13.8 dB) in a broadside radiation than other planar MMW antenna structures such as SIW backed transverse slots, miniaturized slots with single director, dielectric resonator antennas, twin dipole array and other printed antennas.

2. The antipodal fermi linear tapered slot antenna structure, presented for endfire radiation [83], achieved a higher gain (16.4 dB) than previously proposed MMW planar antenna structures such as planar horn antennas, dielectric rod antennas, printed yagi and CPW fed ALTSA. The knife edge corrugation profile for rectangular corrugation is utilized. The cross polarization level is improved along with side lobe levels due to knife edge corrugation profile.

3. Width of AFLTSA is smaller than a wavelength which is beneficial in designing multi-element antenna structures. A novel shape of tapered slot is utilized which allows a higher gain with shorter antenna structure [84].

5.3 Future Scope

This thesis was focused on the single element design of planar antennas achieving high gain at Ka band. These structures can be used in multiple-element systems to cover a larger area. Beam-forming network such as Butler matrix can be used to generate orthogonal beams in azimuth plane. In this method, the elements are placed such that their peaks are in angular separation and their 3 dB beamwidths cross each other [20]. Therefore, one wide beam with high gain of individual elements can be achieved.

References

[1] G. Falciasecca, "Marconi's Early Experiments in Wireless Telegraphy, 1895," *IEEE Antennas and Propagation Magazine*, vol. 52, no. 6, pp. 220–221, Dec. 2010.

[2] A. F. Molisch, *Wireless Communications*, 2nd ed., U.K.: John Wiley & sons Inc., 2011.

[3] P. Bhartia and I. J. Bahl, *Millimeter Wave Engineering and Applications,* Canada: John Wiley & sons Inc., 1984.

[4] W. Huang and A. A. Kishk, "Compact dielectric resonator antenna for microwave breast cancer detection," *IET Microwaves, Antennas Propagation*, vol. 3, no. 4, pp. 638–644, Jun. 2009.

[5] E. Topsakal, "Antennas for medical applications: Ongoing research and future challenges," in *International Conference on Electromagnetics in Advanced Applications. ICEAA '09*, 2009, pp. 890–893.

[6] L. Frenzel, *Communication Electronics: Principles and Applications*. McGraw-Hill Companies, 2001.

[7] "IEEE Standard Definitions of Terms for Antennas," *IEEE Std 145-1993*, pp. 1–32, Jul. 1993.

[8] "Canadian Table of Frequency Allocations 9 kHz to 275 GHz," Industry Canada, Canada, Dec. 2009.

[9] C. E. Shannon, *A Mathematical Theory of Communication*, vol. 27, pp. 379–423, 623–656, 1948.

[10] K. Huang and D. Edwards, *Millimetre Wave Antennas for Gigabit wireless communication*, John Wiley and Sons Inc., 2008.

[11] C. A. Balanis, *Antenna Theory analysis and design*, Third. Ed., USA: John Wiley & sons Inc., 2005.

[12] A. Goldsmith, *Wireless Communications*. USA: Cambridge University Press, 2005.

[13] G. Stuber, *Principles of Mobile Communication*, 3rd ed. Springer, 2011.

[14] T. S. Rappaport, S. Sun, R. Mayzus, H. Zhao, Y. Azar, K. Wang, G. N. Wong, J. K. Schulz, M. Samimi, and F. Gutierrez, "Millimeter Wave Mobile Communications for 5G Cellular: It Will Work!," *IEEE Access*, vol. 1, pp. 335–349, 2013.

[15] "Key ICT indicators for developed and developing countries and the world (totals and penetration rates)." Information and Communication Technology (ICT), 2013.

[16] "Global mobile statistics 2014 Part A: Mobile subscribers; handset market share; mobile operators," Available FTP : *http://mobithinking.com/mobile-marketing-tools/latest-mobile-stats/a#uniquesubscribers*, Jun-2014. .

[17] "Specific attenuation model for rain for use in prediction method," RECOMMENDATION ITU-R P.838-3, 2005.

[18] E-Band Communications, LLC, "E band Technology," Available FTP : http://www.e-band.com/index.php?id=86, 2014.

[19] M. Sumi, K. Komiya, R. Yamaguchi, and K. Cho, "Azimuth pattern design to reduce interference in overlapping sectors using combined tilt," in *2010 IEEE International Conference on Wireless Information Technology and Systems (ICWITS)*, 2010, pp. 1–4.

[20] Z. N. Chen and kwai-man Luk, "*Antennas for Base Stations in wireless communications"*, McGraw-Hill Companies, 2009.

[21] J. F. Ramsay, "Microwave Antenna and Waveguide Techniques before 1900," *Proceedings of the IRE*, vol. 46, no. 2, pp. 405–415, Feb. 1958.

[22] M. Skolnik, *Introduction to RADAR systems*, 3rd ed. Boston: Tata McGraw-Hill Companies, 2001.

[23] S. Preradovic and N. Karmakar, "Chipless millimeter wave identification (MMID) tag at 30 GHz," in *Microwave Conference (EuMC), 2011 41st European*, 2011, pp. 123–126.

[24] K. Mizuno, H. Matono, Y. Wagatsuma, H. Warashina, H. Sato, S. Miyanaga, and Y. Yamanaka, "New applications of millimeter-wave incoherent imaging," in *Microwave Symposium Digest, 2005 IEEE MTT-S International*, 2005, p. 4.

[25] A. Elboushi and A. Sebak, "B14. Active millimeter-wave imaging system for hidden weapons detection," in *Radio Science Conference (NRSC),* 2012, pp. 111–118.

[26] L. Lucci, R. Nesti, G. Pelosi, and S. Selleri, "A Stackable Constant-Width Corrugated Horn Design for High-Performance and Low-Cost Feed Arrays at Millimeter Wavelengths," *IEEE Antennas and Wireless Propagation Letters*, vol. 11, pp. 1162–1165, 2012.

[27] K. Liu, C. A. Balanis, and G. C. Barber, "Low-loss material coating for horn antenna beam shaping," in *Antennas and Propagation Society International Symposium, 1991. AP-S. Digest*, vol.3, 1991, pp. 1664–1667.

[28] N. Ghassemi and K. Wu, "Millimeter-Wave Integrated Pyramidal Horn Antenna Made of Multilayer Printed Circuit Board (PCB) Process," *IEEE Transactions on Antennas and Propagation*, vol. 60, no. 9, pp. 4432–4435, 2012.

[29] H. Wang, D.-G. Fang, B. Zhang, and W.-Q. Che, "Dielectric Loaded Substrate Integrated Waveguide (SIW) -Plane Horn Antennas," *IEEE Transactions on Antennas and Propagation*, vol. 58, no. 3, pp. 640–647, 2010.

[30] S. Methfessel and L. Schmidt, "Design of a balanced-fed patch-excited horn antenna at millimeter-wave frequencies," in *2010 Proceedings of the Fourth European Conference on Antennas and Propagation (EuCAP)*, 2010, pp. 1–4.

[31] B. Pan, Y. Li, G. E. Ponchak, J. Papapolymerou, and M. M. Tentzeris, "A 60-GHz CPW-Fed High-Gain and Broadband Integrated Horn Antenna," *IEEE Transactions on Antennas and Propagation*, vol. 57, no. 4, pp. 1050–1056, 2009.

[32] M. El-Nawawy, A. M. M. A. Allam, and M. Ghoneima, "Design and fabrication of W-band SIW horn antenna using PCB process," in *2013 1st International Conference on Communications, Signal Processing, and their Applications (ICCSPA)*, 2013, pp. 1–4.

[33] S. A. Razavi and M. H. Neshati, "Low profile H-plane horn antenna based on half mode substrate integrated waveguide technique," in *2012 20th Iranian Conference on Electrical Engineering (ICEE)*, 2012, pp. 1351–1354.

[34] S. R. Ranade and D. U. Nair, "Design of a substrate integrated waveguide H plane Horn antenna on a PTFE substrate for automotive radar application," in *2011 IEEE Applied Electromagnetics Conference (AEMC)*, 2011, pp. 1–4.

[35] J. S. Fu, "Preliminary study of 60 GHz air-filled SIW H-plane horn antenna," in *2011 IEEE Electrical Design of Advanced Packaging and Systems Symposium (EDAPS)*, 2011, pp. 1–4.

[36] N. Ghassemi and K. Wu, "Planar High-Gain Dielectric-Loaded Antipodal Linearly Tapered Slot Antenna for E and W Band Gigabyte Point-to-Point Wireless Services," *IEEE Trans. Antennas Propag.*, vol. 61, no. 4, pp. 1747–1755, 2013.

[37] W. Che, B. Fu, P. Yao, Y. L. Chow, and E. K. N. Yung, "A compact substrate integrated waveguide H-plane horn antenna with dielectric arc lens," *International Journal of RF and Microwave Computer-Aided Engineering*, vol. 17, no. 5, pp. 473–479, 2007.

[38] B. Fuchs, O. Lafond, S. Rondineau, and M. Himdi, "Design and characterization of half Maxwell fish-eye lens antennas in millimeter waves," *IEEE Transactions on Microwave Theory and Techniques*, vol. 54, no. 6, pp. 2292–2300, Jun. 2006.

[39] C. Hua, X. Wu, and W. Wu, "A millimeter-wave cylindrical modified Luneberg lens antenna," in *Microwave Symposium Digest (MTT), 2012 IEEE MTT-S International*, 2012, pp. 1–3.

[40] C. A. Fernandes, R. C. Martins, T. Radil, P. M. Ramos, E. B. Lima, C. R. Medeiros, and J. R. Costa, "Low-cost mechanically steered millimeter-wave lens antenna system for indoor LANs," in *2010 International Workshop on Antenna Technology (iWAT)*, 2010, pp. 1–4.

[41] R. E. Collin and F. J. Zucker, *Antenna Theory Part 2*, vol. 7, USA: McGraw-Hill Companies, 1969.

[42] Q. Chen, C. Wang, B. Liu, Q. Sun, and Y. Zhao, "Dielectric step-tapered rod antenna array for millimeter waves," in *2011 36th International Conference on Infrared, Millimeter and Terahertz Waves (IRMMW-THz)*, 2011, pp. 1–2.

[43] S. Xu and X. Wu, "A millimeter-wave omnidirectional dielectric rod metallic grating antenna," *IEEE Transactions on Antennas and Propagation*, vol. 44, no. 1, pp. 74–79, Jan. 1996.

[44] S. Kobayashi, R. Mittra, and R. Lampe, "Dielectric tapered rod antennas for millimeter-wave applications," *IEEE Transactions on Antennas and Propagation*, vol. 30, no. 1, pp. 54–58, Jan. 1982.

[45] Y. Shiau, "Dielectric Rod Antennas for Millimeter-Wave Integrated Circuits (Short Papers)," *IEEE Transactions on Microwave Theory and Techniques*, vol. 24, no. 11, pp. 869–872, Nov. 1976.

[46] R. Kazemi, A. E. Fathy, and R. A. Sadeghzadeh, "Dielectric Rod Antenna Array With Substrate Integrated Waveguide Planar Feed Network for Wideband Applications," *IEEE Transactions on Antennas and Propagation*, vol. 60, no. 3, pp. 1312–1319, 2012.

[47] J. Liu, D. R. Jackson, and Y. Long, "Substrate Integrated Waveguide (SIW) Leaky-Wave Antenna With Transverse Slots," *IEEE Transactions on Antennas and Propagation*, vol. 60, no. 1, pp. 20–29, 2012.

[48] H. Han, Y. Wang, X. Liu, and H. Guo, "Miniaturized high gain slot antenna with single-layer director," in *2013 Proceedings of the International Symposium on Antennas Propagation (ISAP)*, 2013, vol. 01, pp. 265–268.

[49] L. Goldstone and A. A. Oliner, "Leaky-wave antennas I: Rectangular waveguides," *IRE Transactions on Antennas and Propagation*, vol. 7, no. 4, pp. 307–319, Oct. 1959.

[50] P. Lampariello, "New millimeter-wave leaky-wave antennas," in *Microwave Conference Proceedings, 1997. APMC '97, 1997 Asia-Pacific*, 1997, vol. 1, pp. 405–408.

[51] M. K. Brar and S. K. Sharma, "A wideband aperture-coupled pentagon shape dielectric resonator antenna (DRA) for wireless communication applications," in *2011 IEEE International Symposium on Antennas and Propagation (APSURSI)*, 2011, pp. 1674–1677.

[52] Q. Lai, C. Fumeaux, W. Hong, and R. Vahldieck, "60 GHz Aperture-Coupled Dielectric Resonator Antennas Fed by a Half-Mode Substrate Integrated Waveguide," *IEEE Transactions on Antennas and Propagation*, vol. 58, no. 6, pp. 1856–1864, 2010.

[53] W. M. Abdel-Wahab and S. Safavi-Naeini, "Improvement of aperture coupling in SIW-fed DRA using embedded metallic posts," in *2012 IEEE Antennas and Propagation Society International Symposium (APSURSI)*, 2012, pp. 1–2.

[54] G. R. DeJean and M. M. Tentzeris, "A New High-Gain Microstrip Yagi Array Antenna With a High Front-to-Back (F/B) Ratio for WLAN and Millimeter-Wave Applications," *IEEE Transactions on Antennas and Propagation*, vol. 55, no. 2, pp. 298–304, Feb. 2007.

[55] K.-F. Hung and Y.-C. Lin, "Broadband printed circularly-polarised aperture antenna array for millimetre-wave gigabit applications," *Electronics Letters*, vol. 44, no. 25, pp. 1439–1441, Dec. 2008.

[56] Z. Briqech and A. Sebak, "Low-cost 60 GHz printed Yagi antenna array," in *2012 IEEE Antennas and Propagation Society International Symposium (APSURSI)*, 2012, pp. 1–2.

[57] Y.-H. Suh and K. Chang, "A new Millimeter-wave printed dipole phased array antenna using microstrip-fed coplanar stripline tee junctions," *IEEE Transactions on Antennas and Propagation*, vol. 52, no. 8, pp. 2019–2026, Aug. 2004.

[58] R. B. Waterhouse, D. Novak, A. Nirmalathas, and C. Lim, "Broadband printed millimeter-wave antennas," *IEEE Transactions on Antennas and Propagation*, vol. 51, no. 9, pp. 2492–2495, Sep. 2003.

[59] H. Wong, K. B. Ng, C. H. Chan, and K. M. Luk, "Printed antennas for millimeter-wave applications," in *2013 International Workshop on Antenna Technology (iWAT)*, 2013, pp. 411–414.

[60] S. N. Prasad and S. Mahapatra, "A Novel MIC Slot-Line Antenna," in *Microwave Conference, 1979. 9th European*, 1979, pp. 120–124.

[61] P. J. Gibson, "The Vivaldi Aerial," in *Microwave Conference, 1979. 9th European*, 1979, pp. 101–105.

[62] R. N. Simons, R. Q. Lee, and T. D. Perl, "Non-planar linearly tapered slot antennas with balanced microstrip feed," in *, IEEE Antennas and Propagation Society International Symposium, 1992. AP-S. 1992 Digest. Held in Conjuction with: URSI Radio Science Meeting and Nuclear EMP Meeting*, 1992, pp. 2109–2112 vol.4.

[63] D. H. Schaubert, E. L. Kollberg, T. Korzeniowski, T. Thungren, J. Johansson, and K. S. Yngvesson, "Endfire tapered slot antennas on dielectric substrates," *IEEE Transactions on Antennas and Propagation*, vol. 33, no. 12, pp. 1392–1400, 1985.

[64] Z.-C. Hao, W. Hong, J. Chen, X.-P. Chen, and K. Wu, "A novel feeding technique for antipodal linearly tapered slot antenna array," in *Microwave Symposium Digest, 2005 IEEE MTT-S International*, 2005.

[65] F. Taringou, D. Dousset, J. Bornemann, and K. Wu, "Broadband CPW Feed for Millimeter-Wave SIW-Based Antipodal Linearly Tapered Slot Antennas," *IEEE Transactions on Antennas and Propagation*, vol. 61, no. 4, pp. 1756–1762, 2013.

[66] R. Booton, *Computational Methods for Electromagnetics and Microwaves*. USA: John Wiley & sons Inc., 1992.

[67] D. Davidson, "An overview of Computational Electromagnetics for RF and Microwave applications," in *Computational Electromagnetics for RF and Microwave Engineering*, Second., Cambridge University Press, 2011.

[68] T. Hubbing, "Survey of Numerical Electromagneitc Modeling Techniques," University of Mussouri-Rolla, TR91-1-001.3, Sep. 1991.

[69] T. Rylander, A. Bondeson, and P. Ingelstrom, *Computational Electromagnetics*, Second ed., Springer, 2013.

[70] I. Munteanu and T. Weiland, "RF & Microwave Simulation with the Finite Integration Technique- From Component to System Design," in *Scientific Computing in Electrical Engineering*, Springer, 2007.

[71] D. Pozar, *Microwave Engineering*, 3rd ed., John Wiley & sons Inc.,2009.

[72] D. Deslandes, "Design equations for tapered microstrip-to-Substrate Integrated Waveguide transitions," in *Microwave Symposium Digest (MTT), 2010 IEEE MTT-S International*, 2010, pp. 704–707.

[73] K. F. Lee and K. Luk, "Broadbanding Techniques IV - Aperture Coupled Patches," in *Microstrip Patch Antennas*, London: Imperial Colege Press, pp. 291–320, 2011.

[74] F. T. Ulbay, *Fundamentals of Applied Electromagnetics*. USA: Pearson Education Inc., 2004.

[75] Warren Stutzman and G. Thiele, "*Antenna Theory and Design"*, Second. John Wiley & sons Inc., 1998.

[76] D. Deslandes and K. Wu, "Integrated microstrip and rectangular waveguide in planar form," *IEEE Microw. Wirel. Compon. Lett.*, vol. 11, no. 2, pp. 68–70, 2001.

[77] K. Wu, D. Deslandes, and Y. Cassivi, "The substrate integrated circuits - a new concept for high-frequency electronics and optoelectronics," in *6th International Conference on Telecommunications in Modern Satellite, Cable and Broadcasting Service, 2003.*, P–III–P–X vol.1.

[78] J. E. Rayas-Sanchez and V. Gutierrez-Ayala, "A general EM-based design procedure for single-layer substrate integrated waveguide interconnects with microstrip transitions," in *Microwave Symposium Digest, 2008 IEEE MTT-S International*, 2008, pp. 983–986.

[79] F. Xu and K. Wu, "Guided-wave and leakage characteristics of substrate integrated waveguide," *IEEE Trans. Microw. Theory Tech.*, vol. 53, no. 1, pp. 66–73, 2005.

[80] S. Sugawara, Y. Maita, K. Adachi, K. Mori, and K. Mizuno, "A mm-wave tapered slot antenna with improved radiation pattern," in *Microwave Symposium Digest, 1997., IEEE MTT-S International*, 1997, vol. 2, pp. 959–962.

[81] Z. Briqech, A. Sebak, and T. A. Denidni, "60 GHz Fermi tapered slot antenna with sin-corrugation," in *2013 IEEE Antennas and Propagation Society International Symposium (APSURSI)*, 2013, pp. 160–161.

[82] K. Phalak and A. Sebak, "Aperture Coupled Microstrip Patch Antenna Array for High Gain at Millimeter Waves," to be presented at the 2014 IEEE International Conference on Communication, Networks and Satellite, Jakarta, November, 2014.

[83] K. Phalak, Z. Briqech, and A. Sebak, "Ka-Band Antipodal Fermi-Linear Tapered Slot Antenna with a Knife Edge Corrugation," *Microw. Opt. Technol. Lett.*, Submitted, 2014.

[84] K. Phalak, Z. Briqech, and A. Sebak, "Substrate Integrated Waveguide fed Antipodal Fermi Linear Tapered Slot Antenna_at 28 GHz," presented at 16th international symposium on antenna technology and applied electromagnetics, in press, 2014.